BSc Thesis

eVTOL Design, Energy Storage & Charging

4691709 Peer Kalk
4721330 Constantijn Zevenbergen

Delft University of Technology | June 18, 2021

BSc Thesis

eVTOL Design, Energy Storage & Charging

by

Peer Kalk
Constantijn Zevenbergen

Student Number:	4691709	(Peer Kalk)
	4721330	(Constantijn Zevenbergen)
Project Duration:	April 2021 – June 2021	
Thesis Committee:	Dr. ir. G.R. Chandra Mouli,	TU Delft, supervisor
	Dr. J. Dong,	TU Delft
	Dr. D. Cavallo,	TU Delft

EE3L11 Bachelor Graduation Project Electrical Engineering
Faculty of Electrical Engineering, Mathematics & Computer Science

TU Delft

Abstract

As electric vehicles are quickly taking over the automotive industry, electric airplanes are also starting their upswing. With air travel and transport in general being a large polluter of CO_2 gases, the transition to electric flight becomes more prominent every year. This transition is starting small with non-commercial airplanes. Several companies are starting with development of eVTOLs, electric Vertical Take-Off and Landing vehicles. The idea behind them is that they can easily move into and out of the city through the air, speeding up transport and travel in urban areas while keeping CO_2 emissions at the vehicle level at zero.

This thesis, together with two other theses, will elaborate on the design of such an eVTOL. Its design is created by looking at the layout of the propellers, the wings and the fuselage and the internal layout is composed by working out the electric drivetrain from the energy storage to the electric motors and by drafting up the control systems. In specific, this thesis dives into the external design and the internal electric energy storage. It does this by settling on a design and calculating certain specifications, like wing area and propeller and fuselage size. From there the necessary powers and energies are calculated. With these powers and energies, a battery pack is designed together with a battery management system and a charging system. The other two theses will design the propulsion system and the control system of the eVTOL.

The result of the thesis is a theoretical design that states the possibilities of Lithium-Sulfur cells inside an eVTOL. An efficient tandem wing design with fixed wings and fixed rotors makes sure there is a healthy balance between the maximum power and total energy needed to take off vertically and fly 125 kilometers. With the Lithium-Sulfur cells a battery pack is made with its accompanying battery management system that monitors and manages the cells' characteristics. Next to the battery pack, theory on charging and a simplified charging simulation has been done to show that charging in 15 minutes should be possible by the time the eVTOL enters into service.

Preface

This thesis is written in context of the Electrical Engineering Bachelor Graduation Project. The thesis project is derived from a challenge created by the AIAA and IEEE with the goal of designing an eVTOL aircraft. This particular thesis is about the design of the eVTOL and its Energy Storage System, to achieve the design presented in this thesis, we have been doing research and calculations over the span of two months. We delved into the world of aviation, a place we were quite unfamiliar with as electrical engineers, and currently upcoming technologies, which gave us an insight into the technological future. As the eVTOL is supposed to become available in 2030, it is hoped that the presented technology will be used globally by the end of this decade. Creating a faster, more efficient and more environment friendly method of cargo transportation.

We would like to express our sincere thanks to Daniele Ragni, Tomas Sinnige, Wiljan Vermeer, Jianning Dong and Gautham Ram Chandra Mouli for their constant support throughout this project.

P.E.A. Kalk
C.B.J. Zevenbergen
Delft, June 2021

Contents

List of Units and Abbreviations

Units

A_p	Effective Propeller Area [m^2]
A_w	Effective Wing Area [m^2]
a	eVTOL Acceleration [m/s^2]
C_D	Drag Coefficient [-]
C_{D0}	Zero-Lift Drag Coefficient [-]
C_{Di}	Induced Drag Coefficient [-]
C_f	Skin Friction Coefficient [-]
C_l	Lift Coefficient [-]
C_P	Polarization Capacitor [F]
C_t	Battery Capacity [As]
c	Wing Chord [m]
γ	Coulombic Efficiency [-]
η_0	Overall Efficiency [-]
$\eta_{DC/DC}$	DC/DC Converter Efficiency [-]
η_{inv}	Inverter Efficiency [-]
η_m	Motor Efficiency [-]
η_p	Propeller Efficiency [-]
η_Ω	Ohmic Efficiency [-]
f_{tc}	Thickness Ratio Function [-]
f_M	Mach Number Function [-]
i	Current [A]
L	Lift [N]
M	Mach Number [-]
m	Mass [kg]
μ	(Air) Fluid Viscosity [kg/(m·s)]
P	Power [W]
Q	Torque [Nm]
R_p	Propeller Radius [m]
R_0	Ohmic Resistor [Ω]
R_P	Polarization Resistor [Ω]
r	Internal Resistance [Ω]
ρ	(Air) Density [kg/m^3]
S_{wet}	Wetted Area of the Wing [m^2]
T	Thrust [N]
θ	Wing to Body Angle [°]
U_{OC}	Open-Circuit Voltage [V]
v_∞	eVTOL Velocity [m/s]
W	Fusion Gain [-]

Abbreviations

AIAA	American Institute of Aeronautics and Astronautics
BMS	Battery Management System
CCS	Combined Charging System
CC/CV	Constant Current / Constant Voltage
CHAdeMO	Charge de Move
DCFC	Direct Current Fast Charging
EASA	European Union Aviation Safety Agency
ECN	Equivalent Circuit Network
EES	Electrical Energy Storage
EIS	Entry Into Service
EATS	Electric Aircraft Technologies Symposium
EV	Electric Vehicle
FAA	(US) Federal Aviation Authority
FFRLS	Forgetting Factor Recursive Least Square
IEEE	Institute of Electrical and Electronics Engineers
Li-S	Lithium-Sulfur
LFP	Lithium Iron Phosphate
LMO	Lithium Manganese Oxide
MTOW	Maximum Take-Off Weight
NASA	National Aeronautics and Space Administration
NCA	Lithium Nickel Cobalt Aluminium Oxide
NMC	Lithium Nickel Manganese Cobalt Oxide
RPM	Revolutions Per Minute
SMES	Super Magnetic Energy Storage
SOC	State-of-Charge
SOH	State-of-Health
SVM	Support Vector Machine
UAM	Urban Air Mobility
UAS	Unmanned Aircraft Systems
UAV	Unmanned Aerial Vehicle
UPS	Uninterruptible Power Supply
V2X	Vehicle-to-Everything

1 Introduction

Since the last century, the aeronautics industry is in the middle of another revolution. First, environment awareness is becoming more prominent, providing a push towards the reduction of harmful emissions and the overall environmental footprint of the aviation industry. Secondly, new needs and trends are currently evolving towards (more) autonomous aircraft to prepare for a future without pilots.

Within the aviation scene, the reduction of weight and fuel consumption has been high on the agenda, all to be able to improve performance. Trying to find solutions to force these reductions, new ideas and concepts have been rising. For the development of the Urban Air Mobility (UAM) sector, the new main contender is the electric Vertical Take-Off and Landing (eVTOL) aircraft. UAM is an alternative way of intra-city passenger transportation without using any roads, being researched and developed by government, academia and industry. The concept of short-haul passenger air trips can be achieved by technological advances such as electrical power transmission, battery storage, control systems and propulsion systems. The concept will introduce a more reliable, safer and more environmental friendly alternative to current (aviation) transport methods. The electric flying car, something that always seemed unreal, is starting to become reality and many businesses are already testing their design. Numerous start-ups and established players are currently working on earning their place within the UAM sector by creating an eVTOL. However, performance and autonomy of the eVTOL are still limited by what is possible today.

Currently, interesting state-of-the-art competition are teams like Lilium [1] and Blackfly [2]. Blackfly has an eVTOL that weighs 155 kilograms and can carry an additional 90 kilograms for a distance of 65 kilometers. An eVTOL that is slightly larger and more focused on cargo is the Airbus CityAirbus [3] which has a maximum take-off weight of 2200 kilograms and can reach a distance of around 100 kilometers.

The main question is how far the performance can evolve in the current decade, taking into account the technological progress. Despite the developments with the eVTOL, urban air mobility is constrained by many aspects to this day. Regulations, air traffic control, infrastructure availability and community acceptance currently withhold the expansion of this sector. A lot can and will change over the coming years, so it will be interesting to watch the developments within the UAM sector and especially the advances of the concept of eVTOLs [4] [5].

1.1. Project Objective

This thesis has been derived from a challenge [4], composed by the AIAA and the IEEE which states the following question: What is the max payload, in kilograms, that can be achieved for an eVTOL aircraft, with no CO_2 emission by the vehicle, according certain specifications? The relevant specifications are stated in chapter 2. To participate in the challenge a report had to be written of a maximum of 30 pages stating the following information;

- **The Aircraft Design Considerations**, including a general description of the architecture (shape, length, wingspan, amount of propellers, etc.) and how the electric powertrain is integrated into the eVTOL,
- **The Electric Propulsion System Design**, which includes the system for power generation, energy storage and power distribution, all with details up to voltages, currents, torques, etc.,
- **Concepts of Operation**, for which flight management, a passenger or cargo consideration and energy refill strategy are included.

For all of the systems it is important that weights are included, as that is the main object of the challenge.

The idea that lies behind this challenge is that an electric VTOL is an upcoming concept and has not been designed often before. There are several ways to take off vertically, but not many VTOL designs have yet been focused on lifting large amounts of weight compared to the empty weight of the aircraft. That is the first part where the challenge lies for the team, because the eVTOL will have to be designed in such a way that the power and energy needed do not outweigh each other. In other words, the design should not consume extreme amounts of power while taking off vertically, but it should also not have large amounts of drag during horizontal flight and both affect each other. The design encapsulates specifically an *electric* VTOL, which advances the largest part of the challenge, as both the electric energy storage and electric motors, as well as the entire power system have to be optimized for both vertical and horizontal flight.

Keeping in mind the aforementioned optimization of power and energy, an electric energy storage can be constructed with many types of energy storage. One type may favour high power and the other may favour high energy. Bring into the mix that the electric motors and accompanying motors also favour different torques, currents and voltages and a real optimization challenge arises. That is exactly what this thesis and the two accessory theses are about.

This thesis focuses on the design of the eVTOL and its electric energy storage system. Figure A.7 shows the division of focus within the three teams, established to achieve the most efficient design possible within the given time span. As can be seen, the energy storage team focuses on the battery pack with its according BMS, DC/DC Converter and charging system. The design of the eVTOL is not integrated in the diagram, but it will be discussed in-depth in this thesis as well. The two main objectives that are thrived for in this thesis are the following; what is the most weight efficient electric energy storage system for an eVTOL with given specifications and give design specifications of an eVTOL that has to fulfil the requirements as stated by the challenge. The first will be achieved by designing a battery pack with BMS and charging solution. The second will be gained through making calculations on total wing specifications, fuselage dimensions, propeller specifications and other aircraft ratios.

1.2. Thesis Outline

To start, chapter 2 lists the program of requirements for different parts of the project. Next, chapter 3 will be about the design of the eVTOL. The general shape, the size and amount of the propellers, the wings and the fuselage will be discussed there. With the design of the eVTOL decided, the energy and power demand can be determined in chapter 4. Also the efficiencies of all the powertrain components are included to find a specific estimation of the power and energy that the energy storage system has to provide. This energy storage system is designed in chapter 5 where firstly several types of energy storage are mentioned to finally settle on one of them. With this type of energy storage a broad design is made in the same chapter to eventually create one pack for the energy storage system. chapter 6 is devoted to the charging of this pack and will mention current charging options and future perspectives in charging. It will also mention how the chosen storage type can be charged most efficiently. In chapter 7, a management system for the pack is designed. Its design will make sure that the pack stays healthy by monitoring and managing where necessary and it will also give some estimation methods. At last, chapter 8 provides a conclusion on the design, together with recommendations on future work. Appendix A provides an overview of all eVTOL renders, schematics, block diagrams and plots referred to throughout the thesis, Finally, Appendix B provides all the Matlab code used for all the calculations and plots.

2

Program of Requirements

The main goal of the eVTOL project as described in the introduction, chapter 1, is to maximize the payload of an eVTOL aircraft. As stated by the IEEE, there are several requirements connected to the design proposal. To optimize the design of the eVTOL, the work has been divided in three subgroups with some parts completed by the entire group. The requirements for the entire project can be divided in several parts containing the general requirements and the requirements per subgroup. The division of the subgroup with their different parts can be seen in Figure A.7. As explained earlier, this thesis will focus on the eVTOL Design and Energy Storage System. The requirements in the following sections will be used for assessment of the design and results presented throughout this thesis. First an overview of the general requirements for the eVTOL of the project will be given, these requirements hold for all the subgroups. Next, the requirements will be listed that are of importance especially for this thesis.

2.1. General

The eVTOL from the submitted design proposal must posses the following:

- A range of 100 kilometers with a 25 kilometers backup,
- A cruise speed of 250 km/h,
- An operating altitude relative to the ground of 150 meters, and a maximum altitude above sea level of 1070 meters,
- An aircraft planform dimension which should fit within a 15-meter diameter circle,
- A Maximum Take-Off Weight (MTOW) of 2500 kilograms,
- An anticipated Entry into Service (EIS) of 2030,
- An electric propulsion system which must produce zero CO_2 at the vehicle level.

2.2. Design

The requirements for the eVTOL Design part are presented next:

- Large enough wings to be able to lift 2500 kilograms at a velocity of 250 km/h,
- A large enough propeller radius and amount to be able to accelerate 2500 kilograms at 3 m/s^2,
- A large enough fuselage to carry the largest possible payload,
- A aerodynamic aircraft design, with adequate lift and drag coefficients.

2.3. Energy Storage

The following requirements hold for the Energy Storage System of the eVTOL:

- Enough power to be able to accelerate 2500 kilograms at 3 m/s^2,
- Enough energy to take-off vertically, cruise horizontally and land vertically with a total distance of 125 kilometers
- A high enough voltage to be able to drive the right motor RPM,
- A high enough current to be able to drive the right motor torque,
- A description of a Battery Management System,
- A description of a charging system.

3

eVTOL Aircraft Design

3.1. Description & Architecture eVTOL

The general design of the eVTOL can be described as a fixed-wing, fixed-rotor tandem wing aircraft. Fixed-wing, fixed-rotor means that there are no rotating parts on the plane, other than the rotors, so neither the wings nor the motors tilt. A tandem wing means that there are two wings connected to the fuselage. In particular, for this eVTOL, the wings will not be at similar heights, seen from the front when flying horizontally, so the wings will be at an angle, compared to the body. This will minimize the effects that the front propellers and wing will have on the rear propellers and wing as the propellers are fixed perdendicular to the wings. Now, this will create a very rough shape for the airplane, but in order to find more specific requirements on power and energy demand for the energy storage, more specifications have to be determined, such as the propeller radius, the wing-to-body angle, the wing area and the fuselage size. Hence, this chapter is devoted to determining all the important eVTOL design aspects. To get a clear insight of the design of the eVTOL, renders are shown in Appendix A.

3.2. Propeller Specifications

A propeller can be designed in many ways. Aspects of a propeller can be angles like the twist and pitch, its size, the rotation velocity and, additionally in the case of this eVTOL, the total amount of propellers installed on the eVTOL. The rotation velocity and angles of the propellers will be defined by the Propulsion Team, so they are not covered in this Section. Next to that, the propulsion Team has already defined the amount of propellers to be at least eight propellers. This is needed to keep the symmetry of the eVTOL in terms of amount of propellers per side of a wing, but to also achieve a good redundancy where 25% of the motors can fail. That leaves the size of the propellers and whether eight propellers will suffice the requirements to be determined in this section.

3.2.1. Propeller Radius

To define the propeller radius, the momentum theory [6] is used which states the following Equation.

$$P = \sqrt{\frac{T^3}{2\rho A}} \tag{3.1}$$

Where P is the power delivered to the propeller's axis, T is the required thrust, ρ is the air density (1.225 kg/m^3 at sea level) and A_p is the area of the propeller disk, so $A_p = \pi \cdot R^2$, where R is the propeller radius. In a more resolved calculation, where different flight states are added, for the maximum power and required energy for an entire flight, the radius of the propeller in a setup with eight propellers would look like the graphs in Figure 3.1. An obvious conclusion that can be drawn from this is that the propellers should be as large as possible to decrease the amount of power needed for certain thrusts and thus also decrease the amount of energy needed on the aircraft. However, the aircraft design is limited in a way that it has to fit within a circle with a diameter of 15 meters. Hence, the propeller radius is defined to be 1.5 meters such that there is a little bit of play in the length of the fuselage later on (up

to six meters in length). Also, much larger propellers would require too much torque from the motors, so 1.5 meters is a good radius to settle for. The power needed in Figure 3.1 at a radius of 1.5 meters is equal to approximately 850kW. This means that eight propellers should work for this design.

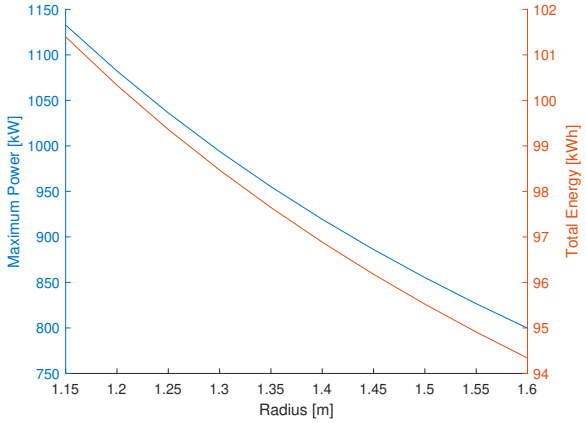

Figure 3.1: Power and Energy Demand with Different Propeller Radii

3.3. Wing Design

The next important aspects to design are the size and shape of the wing. They will mainly determine the lift and drag in horizontal flight (cruise).

3.3.1. Wing Area

The wing area will follow from the amount of lift that needs to be created by the wing to keep the eVTOL at an even altitude during cruise. To calculate this area, the lift equation [7] is used.

$$L = \frac{1}{2} C_l \cdot \rho \cdot v_\infty^2 \cdot A_w \tag{3.2}$$

Where L is the lift force generated by the wing, which needs to be equal to the gravitational force, $2500\,kg \cdot 10\,m/s^2$, to cancel the gravitational force, C_l is the lift coefficient, ρ is the air density, v_∞ is the eVTOL velocity, equal to $69.5\,m/s$, and A_w is the area of the wing. Everything in this equation is known for the eVTOL at cruise, apart from C_l and A_w, so after rewriting the Equation, A_w can be estimated such that C_l achieves a reasonable value. Such a reasonable value is in this case said to be slightly below 0.5 ([8]), which gives a reasonable value for A_w to be 20 m^2. With this A_w, C_l is defined to be equal to 0.42.

3.3.2. Wingspan and Chord

With this wing area, the wingspan and wing chord can now be determined. As said before, there are two wings on the eVTOL and as the main focus of the project is around electronics, the wing planform will be kept as simple as possible. Additionally, the front and rear wings will have the same area and wingspan and on top of that the wings will be rectangular for the sake of simplicity in calculations. Rectangular wings are generally undesirable as this increases the drag, but it does make the drag calculations much simpler [9, p. 69].
A frequently used design specification of an aircraft is the aspect ratio (AR), defined by $AR = b^2/A_w$ where b is the wingspan and A_w is the wing area. This AR will later on also be used to calculate drag during cruise. To calculate that drag, the AR needs to be greater than six, as explained by [9, p. 69]. As a result, the wingspan is determined to be 11.5 meters and to keep the same wing area, the wing chord then has to be 0.87 meters. The total aspect ratio is then equal to 13.2, which is twice 6.6 (slightly larger than six), a result from the design having two wings.

3.3.3. Drag of the Wings

The drag is composed of two parts; the induced drag and the zero-lift drag. These drags will later on be used to calculate the thrust needed to keep the eVTOL flying at a constant cruise velocity. The general

equation to calculate drag is defined by [9, p. 63]:

$$D = \frac{1}{2} C_D \cdot \rho \cdot v_\infty^2 \cdot A_w \tag{3.3}$$

Where D is the drag force, C_D is the drag coefficient, ρ is the air density, v_∞ is the eVTOL velocity and A_w is the wing area. This equation is similar to Equation 3.2 since the lift and drag forces are normalized with the same quantities to achieve the drag and lift coefficients. So, the lift coefficient has been swapped out for the drag coefficient. Now, to calculate the drag, the drag coefficient for the wing has to be defined. Equation 3.3 works for both the induced drag as for the zero-lift drag, but they both have different drag coefficients. For now, the induced drag coefficient will be denoted by C_{Di} and the zero-lift drag coefficient as C_{D0}.
To find C_{Di}, the equation from [9, p. 69-70] is used which states the following.

$$C_{Di} = K \cdot C_l^2 \tag{3.4}$$

Where

$$K = \frac{1}{\pi \cdot e \cdot AR} \tag{3.5}$$

And where

$$e = 1.78(1 - 0.045 \cdot AR^{0.68}) - 0.64 \tag{3.6}$$

Filling in the AR and the previously found C_l, these equations state that $C_{Di} = 0.0100$, 100 drag counts. The induced drag that then follows from this C_{Di} equals 590N.

To find C_{D0}, the equation from [9, p. 74-76] is used.

$$C_{D0} = C_f \cdot f_{tc} \cdot f_M \cdot \frac{S_{wet}}{A_w} \left(\frac{C_{Di}}{0.004} \right)^{0.4} \tag{3.7}$$

Where C_{D0} zero-lift drag Coefficient, C_f the skin friction coefficient, f_{tc} the function of thickness ratio, f_M the function of the Mach number, S_{wet} the wetted area of the wing, A_w the wing area and C_{Di} the induced drag coefficient.
This equation consists of many unknowns, which are calculated accordingly:

$$C_f = 1.327 \sqrt{\frac{\mu}{\rho \cdot v_\infty \cdot c}} \tag{3.8}$$

Where μ is the fluid viscosity of air ($1.81 \cdot 10^{-5}$ (kg/(m·s)), ρ is the air density, v_∞ is the eVTOL velocity and c is the wing chord. Next:

$$f_{tc} = 1 + 2.7 \left(\frac{t}{c} \right)_{max} + 100 \left(\frac{t}{c} \right)_{max}^4 \tag{3.9}$$

Where $\left(\frac{t}{c} \right)_{max}$ is the maximum thickness to chord ratio of the wing. For the simple wing that is being used in this eVTOL the chord and the maximum thickness are constant over the entire wing and such this ratio is assumed to be 0.2 ([8]). And:

$$f_M = 1 - 0.08 \cdot M^{1.45} \tag{3.10}$$

Where M is the Mach number which can be derived by $M = v_\infty / a_0$ where v_∞ is the eVTOL velocity and a_0 is the speed of sound (343 m/s).
At last, S_{wet}/A is the ratio of the wetted area to the net area of the wing. The wetted area is the area that is entirely in contact with air, so this ratio is assumed to be approximately equal to 2.
Putting this all together gives a value of 0.0032, 32 drag counts, for C_{D0}. The zero-lift drag that then follows from this C_{D0} equals 189N.

3.4. Wing to Body Angle

As the body of the eVTOL will be flying at an angle during cruise, the size and shape of the fuselage matters a lot to the drag that it experiences. Also this angle between the wing and the body can have a large impact on the frontal area of the fuselage, also increasing the drag with a higher wing to body angle. The wing to body angle is defined in a way that it is equal to zero degrees when the wings and the body are parallel to each other and is equal to 90 degrees when the wings are perpendicular to the body. The latter can also be seen as the propellers facing straight up into the air while the body is laying flat on the ground because the propellers are always fixed in a perpendicular orientation to the wings. To define the eventual wing to body angle, first the size of the fuselage needs to be determined, so that the angle can be optimized accordingly.

3.4.1. Fuselage Design

The size of the fuselage should be minimized to keep the drag down as much as possible. Of course, the fuselage should still be large enough to fit a payload. As the Maximum Take-Off Weight (MTOW) should be no larger than 2500 kilograms, an assumption can be made on how much of that weight can be used for the payload. An eVTOL that has a comparable design to this one, is the Opener Blackfly [2]. This eVTOL has an empty weight of 142 kilograms and can take a payload of 113 kilograms. This means that it has a payload to maximum weight ratio of 44%. Comparing this to the 2500 kilograms MTOW, a good estimation for the payload would be that it is equal to approximately 1000 kilograms. This is a very rough estimation and can be optimized by looking at the structural and aerodynamic efficiencies in a later stage.

To convert this payload into a reasonable volume requires the density of products that would most likely be transported by this eVTOL. Densities for many foods can be found in [10] where the densities of many products are described. Let's take, for example, green beans which have a density of 0.53 kg/L, one of the lower densities in the list. Converting this density, together with the 1000 kilograms payload into a volume for the fuselage, results in 1.9 m^3. Very roughly adding another 50% to accommodate for the internal electronics, such as the energy storage and control systems, would add up to approximately 2.9 m^3 and should be plenty enough for the cargo. Again, this is a very rough estimation.

The length for the fuselage depends mainly on the restraint of the 15 meter diameter circle. With the wingspan being equal to 11.5 m and the propeller radius equal to 1.5 m, the fuselage cannot be much longer than 5 meters. To maximize the usage of space and minimize the amount of drag and the weight, it is therefore determined that the fuselage has a length of 5 meters. Assuming the fuselage has approximately the shape of a rectangular box, the length of the sides that is now needed to achieve the approximate 2.9 m^3 would be equal to 0.75 meters.

The only problem is that a square box creates a lot of drag, so this will not be the eventual shape. The shape will approximately be like a mix of a droplet and ellipse seen from the front while laying down. In [11] the drag coefficient of a helicopter is estimated. As a helicopter also has different angles of attack, it is fairly comparable to the drag coefficient of this eVTOL. The paper mostly finds drag coefficients converging around a value of 0.1, so that is also the value that will be used to estimate the drag. The exact drag cannot be calculated yet, because the wing to body angle first has to be defined.

3.4.2. Lying to Vertical Take-Off Power

Up until now it has only made sense to decrease the wing to body angle as much as possible, basically up until the point that the wings are parallel to the body, just like a normal airplane. There are two downsides to this however. First of all, when the wings are parallel to the body, the propellers are facing forward when the eVTOL is laying on the ground. This is a problem, because this way the eVTOL is never going to take off vertically. Secondly, when the wings are parallel to the body, the propellers will be situated right behind each other during cruise which creates unwanted effects. More on the latter will be discussed later.
As the wing to body angle increases, the maximum power needed to get the eVTOL from its laying position to its vertical position decreases exponentially. This behaviour can be seen in Figure 3.2a. The values in these graphs already take into account that, during cruise, the drag increases with a

higher angle. As can be seen, there is a crossover point, so a choice could me made to settle for an angle where a compromise is made. However, another option could be to never let the eVTOL go to a laying position by attaching landing gears to it. A schematic of how this would be implemented can be seen in Figure A.6. Figure 3.2b shows how landing gears can decrease the demand of maximum power and still keep the same energy demand for any landing gear. Hence, the choice is made to include landing gear that can keep the eVTOL in a somewhat vertical position, even when it is not being used.

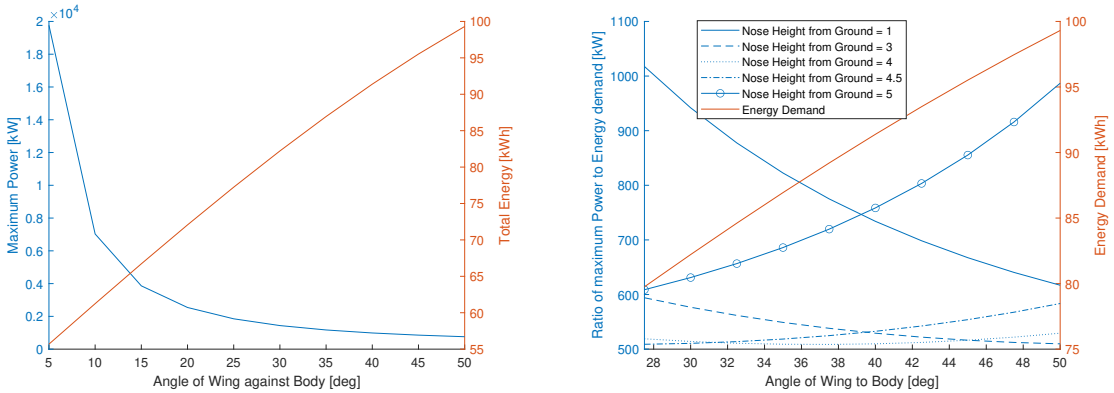

(a) Demand with different Wing to Body Angles

(b) Demand with different Wing to Body Angles and Landing Gears

Figure 3.2: Power and Energy Demand with different Wing to Body Angles

3.4.3. Propeller Overlap

There is still one way to find the best wing to body angle and that is by decreasing the angle so far that the front and rear propellers do not overlap when seen from the front during cruise. The dimensions have been drawn in Figure 3.3. To describe the overlap, the fraction dy/R_p is used. This fraction relates the lateral distance between the wings to the radius of the propellers. This means that when this fraction is equal to two, it is exactly at the point of no overlap. Furthermore w and l are the width and length of the fuselage, respectively, θ is the wing to body angle and c is the wing chord.

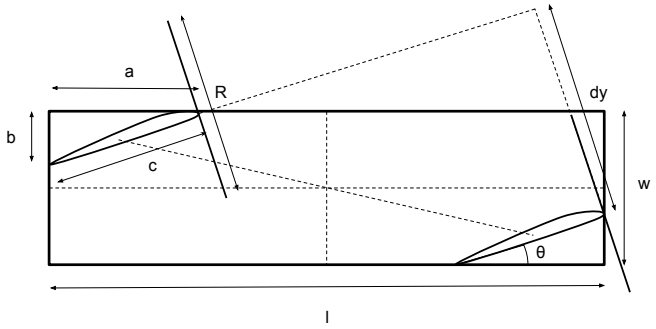

Figure 3.3: Schematic Drawing from the Side of the eVTOL

In [12], dy/R_p is used to determine the influence that one propeller can have on another, laterally. The paper explains how the power consumption of the propellers changes when the overlap increases. A significant increase is found for dy/R_p < 2. This is why the choice is made to not let the propellers overlap.

Figure 3.4 shows the relation between the wing to body angle and dy/R_p. This line is drawn for two setups, one which is the same as in Figure 3.3 and one where the two wings are at a similar height. It also shows a line that is constant at $dy/R_p = 2$. The line where the front wing is situated lower has values that aim slightly more towards a lower angle, which is preferred. That is why the setup with the wings at two different heights is used. The point where this line crosses with $dy/R_p = 2$, is around $\theta = 37°$. This is why the wing to body angle is determined to be equal to $37°$.

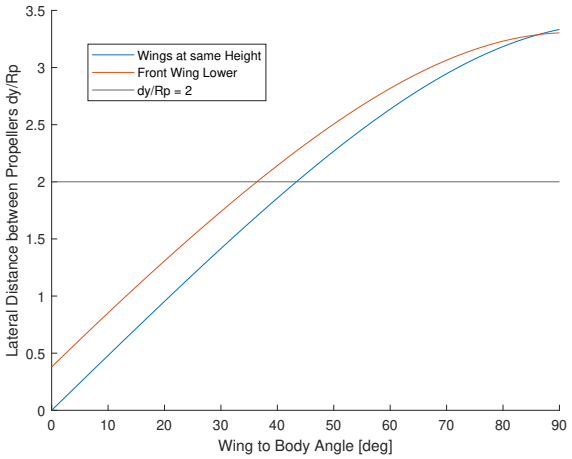

Figure 3.4: Graph relating dy/R_p to the Wing to Body Angle

Using the previously found wing to body angle and the wing chord, a and b in Figure 3.3 can be defined and with the fuselage width and fuselage length the angle for vertical and horizontal flight can then be determined. This angle is found to be slightly higher, situated at $40°$.

3.5. General Overview of eVTOL Design Specifications

All the important aspects of the design have now be determined such that calculations on the energy and power demand can be made. The specifications for the design are summarized in Table 3.1 and an overview of all the different weights can be seen in Table 3.2. Many of these weights have been determined by the Propulsion team. Some additional weight has been added for things like cabling, small electronics, antennas and other aircraft parts. Everything together adds up to an empty weight of 1500 kilograms.

Table 3.1: Overview of the Design Specifications of the eVTOL

Variable	Value	Variable	Value
Total Wing Area	$20\ m^2$	Radius Propellers	$1.5\ m$
Wing Span	$11.5\ m$	Amount of Propellers	8
Wing Chord	$0.87\ m$	Wing to Body Angle	$37°$
Fuselage Length	$5\ m$	Wing Aspect Ratio	13.2
Fuselage Width	$0.75\ m$	Taper Ratio	1

Table 3.2: Weight of all eVTOL Components

Component	Weight [kg]	Amount
Wing Skin	130	2
Fuselage Skin	100	1
Wing Structure	90	2
Fuselage Structure	120	1
Landing Gear	50	1
Electrical Energy Storage	351	1
DC/DC Converter	2.5	2
Motor	28	8
Propeller	10	8
Inverters	4	8
Additional	98	
Total	1500	

4

Energy and Power Demand

With the determined design, the power and accompanying energy for all states can be derived. The main three states that the eVTOL will be in during flight are vertical take-off, horizontal flight (cruise) and vertical landing. The transitions between these states are modeled in a way that there is a linear power transition for which the time is calculated, depending on acceleration, altitude and/or velocity.

4.1. Vertical Take-Off

During vertical take-off there are two forces that have to be canceled, firstly the gravitational force with upwards acceleration and secondly the drag flowing over the wings created by the propeller backwash.

4.1.1. Power Demand

The power needed to accelerate upwards vertically is calculated with Equation 3.1. The upwards thrust in this case is equal to the downwards forces. The downwards gravitational force is equal to $m \cdot (g + a)$ where m is the mass of the eVTOL, g is the gravitational constant and a is the upwards acceleration. An upwards acceleration of 3 m/s^2 has been chosen, which makes the gravitational force equal to $2500 \cdot 13 = 32500N$. The downwards pointing drag force over the wing, created by the propellers backwash, depends on the total thrust as well. The drag can be calculated using Equation 3.3 and the velocity over the wing in this equation can be determined by using Equation 4.1.

$$v_i = \sqrt{\frac{T}{2 \cdot \rho A_p}} \tag{4.1}$$

Where v_i is the induced velocity created by the propeller, T is the thrust the propeller creates, ρ is the air density and A_p is the area of the propeller disk. As this equation depends on the total thrust, but it also is part of the calculation to determine the total thrust, this value can only be calculated through trial and error. This is done by taking values for the total thrust and then defining whether the upwards acceleration is larger than 3 m/s^2. This total thrust already contains the 32500 N that had been determined before and, including the drag, this total thrust is found to be 32969 N. Converting this thrust into power is done by using the momentum theory of Equation 3.1 and gives a total power equal to 528 kW.

4.1.2. Energy Demand

The eVTOL cruises at an altitude of 150 meters. As the eVTOL needs to have no vertical acceleration during cruise, it should stop accelerating halfway this altitude at 75 meters. With an acceleration of 3 m/s^2 it takes five seconds to reach this altitude. At this altitude the eVTOL will go into transition where it will accelerate horizontally with an acceleration of 3 m/s^2 until it has reached a velocity of 69.4 m/s. It will also decelerate vertically with 3 m/s^2 until it has reached an altitude of 150 meters. To reach a velocity of 69.4 m/s with an acceleration of 3 m/s^2 it takes approximately 23 seconds.

During the vertical acceleration approximately $528 \cdot \frac{5}{3600} = 0.7kWh$ is used. The energy during the transition is also dependent on the power during cruise.

4.2. Horizontal Flight

The horizontal flight is also called the cruise. The eVTOL cruises with a velocity of 69.4 m/s. During this cruise it has to overcome all drag that is created by all the parts of the plane.

4.2.1. Power Demand

The thrust that should be created to fly at a constant velocity, should be exactly equal to the sum of all the drag forces. The drags for the wing have already been determined in chapter 3. The drag of the fuselage can be calculated by using Equation 3.3 and the drag coefficient that has been determined in chapter 3.
The frontal area of the fuselage depends on the previously found wing to body angle. With the angle being 37°, the frontal area equals 2.26 m^2. Together with the drag coefficient of 0.1 the zero-lift drag for the fuselage equals 668 N. Adding up the three main drag forces gives a total of $668 + 590 + 189 = 1447N$. Both the zero-lift drags do not add up to the total zero-lift drag, however, so two thirds of this force is added, as they are assumed to be approximately 60% of the total by [9]. This gives a total drag force of approximately 2000N.
To find the power associated with this force, the momentum theory cannot be used as the eVTOL is flying at a high velocity. In stead, the force is multiplied with the velocity of the eVTOL giving a power of $2000 \cdot 69.4 \approx 140kW$

4.2.2. Energy Demand

The energy that is being used by the eVTOL over an entire flight largely depends on the distance of the flight. As the eVTOL cruises with a velocity of 250 km/h, it would cruise for around 30 minutes on a flight of 125 kilometers, whereas it would cruise for around five minutes on a flight of 20 kilometers. With the power of 140 kW during cruise 100 kilometers would thus use $140 \cdot \frac{30}{60} \approx 70kWh$ and 20 kilometers would use $140 \cdot \frac{5}{60} \approx 12kWh$.

4.3. Vertical Landing

Before landing vertically the eVTOL first has to slow down, this is the retransition stage. It will decelerate with 2 m/s^2, which means the retransition takes approximately 35 seconds. During the last few seconds it will slowly accelerate downwards until it is 75 meters above the ground after which it will start to decelerate downwards so it hits the ground smoothly with zero velocity. This landing takes approximately 10 seconds total.

4.3.1. Power Demand

The vertical landing uses the same formulas as those that were used for the vertical take-off, but with different accelerations. Firstly, the eVTOL will accelerate downwards with 2 m/s^2 which needs 255 kW. Afterwards is will decelerate with 2 m/s^2 which needs 470 kW.

4.3.2. Energy Demand

The acceleration and deceleration downwards both take around six seconds as it will accelerate until exactly halfway down and then decelerate with the same acceleration. With the previously determined powers the energy that will be used during this state will be a total of $255 \cdot \frac{6}{3600} + 470 \cdot \frac{6}{3600} \approx 1.3kWh$.

4.4. Total Energy Consumption

The total power an energy that the energy storage system must provide will be higher than the aforementioned values due to efficiencies. The efficiencies and resulting power and energy consumption for different states are therefore determined here.

4.4.1. Efficiencies

$$\eta_0 = \frac{Flow\ Power}{Battery\ Power} = \frac{Battery\ Power}{Chemical\ Power} \cdot \frac{Converter\ Power}{Battery\ Power} \cdot \frac{Inverter\ Power}{Converter\ Power} \cdot \frac{Motor\ Power}{Inverter\ Power} \cdot \frac{Flow\ Power}{Motor\ Power} \tag{4.2}$$

Which is equal to

$$\eta_0 = \eta_\Omega \cdot \eta_{DC/DC} \cdot \eta_{inv} \cdot \eta_m \cdot \eta_p \tag{4.3}$$

Where η_0 is the overall efficiency during horizontal flight, η_Ω the battery ohmic efficiency, $\eta_{DC/DC}$ the DC/DC converter efficiency, η_{inv} the inverter efficiency, η_m the motor efficiency and η_p is the propulsive efficiency.
Table 4.1 shows the efficiencies for different components in different flight states. The efficiencies for the propeller, the motor and the inverter were determined by the propulsion team. Note that the propeller has a figure of merit in stead of an efficiency in static (vertical) flight. The DC/DC converter will be discussed in chapter 5, but its efficiency will already be mentioned in this chapter. The table also includes a factor for the error which takes into account less significant, additional efficiencies and figures of merit. These efficiencies are, for example, thermal efficiencies in the battery, resistive efficiencies in the cables and BMS losses and it also accounts for energy that is being used by electronics for the control of the eVTOL.
In chapter 5 a battery cell is chosen for the energy storage system and the pack, consisting of these cells, its efficiency will already be calculated in this chapter. The ohmic efficiency of the battery is dependent on the internal resistance of the cells. One cell has an internal resistance r and the pack has several cells in series and in parallel, adding up to a resistance of $52 \cdot r$. To calculate the efficiency of this pack at different currents, Equation 4.4 is used.

$$\eta_\Omega = 100\% \cdot \left(1 - \frac{I \cdot 52 \cdot r}{V}\right) \tag{4.4}$$

Where η_Ω and r are the aforementioned ohmic efficiency and internal resistance of a cell, respectively, I is the output current of the battery pack and V is the output voltage of the battery pack, which is equal to 718 V for this pack. [13] states that similar cells to the ones that are mentioned in chapter 5 have an internal resistance of $5 - 15m\Omega$, depending on the SOC. Above an SOC of 20% the internal resistance is relatively constant and closer to $5m\Omega$ than to $15m\Omega$. As the used battery cell is still being researched thoroughly and the paper is from 2016 and the EIS of the eVTOL is in 2030, this internal resistance is estimated to be half at $2.5m\Omega$. The currents are defined by multiplying the power for every state with the already found efficiencies and dividing this value with the voltage of 717 V. The resulting values for the ohmic efficiency of the battery are placed in Table 4.1.

Table 4.1: Efficiencies in the Three Main States of a Flight

	Propulsion		Power Electronics		Battery	Error	Total
State	η_p	η_m	η_{inv}	$\eta_{DC/DC}$	η_Ω	Factor	η_0
Take-Off	0.70	93%	97%	98%	85%	0.95	50%
Cruise	82%	93%	96%	99%	97%	0.95	66%
Landing	0.70	93%	97%	98%	90%	0.95	53%

The overall efficiency η_0 is used to define the total energy used. To determine the maximum power, the ohmic efficiency η_Ω is not taken into account, as it is assumed that manufacturers already take into account their own efficiency when stating a maximum cell power in their datasheet. This gives the following values for the maximum power and total energy used in the three states. (For $\frac{X}{Y}$, X is the maximum power/energy and Y is the efficiency factor, for power the battery efficiency is omitted).

- During **Vertical Take-Off** the maximum power equals $\frac{528}{0.59} \approx 900kW$ and the total energy used is $\frac{0.7}{0.5} \approx 1.4kWh$.
- During **Horizontal Flight** the maximum power equals $\frac{140}{0.68} \approx 190kW$ and the total energy used is $\frac{70}{0.66} \approx 106kWh$ for a flight of 125 kilometers and $\frac{12}{0.66} \approx 18kWh$ for a flight of 20 kilometers.
- During **Vertical Landing** the maximum power in the first part equals $\frac{255}{0.59} \approx 430kW$ and in the seconds part it equals $\frac{470}{0.59} \approx 800kW$ and the total energy used is $\frac{1.3}{0.53} \approx 2.5kWh$.

This means that the maximum power that the energy storage should be able to provide equals 900 kW and the total energy for a 125 kilometer flight, including transition states, equals approximately 116 kWh. These two values will be what the energy storage will be designed around.

5

Energy Storage

Nowadays, there are many ways to store energy all with other technical characteristics, applications and deployment statuses. Electrical Energy Storage (EES) refers to the process of storing electrical energy from a (power) network into a form that can be later converted back to electrical energy when it is needed again. This enables electrical energy to be produced at times of low generation cost, low demand or from intermittent energy sources and later to be used at times of high generation cost, high demand or when no other source is available. Likewise, energy will be generated and stored when on the ground and consumed when flying with aviation applications. With an eVTOL or other electric aircraft it is preferred to have as much energy as possible on board for the least amount of weight when flying to optimize the range and power used [14]. This section will consider multiple applicable solutions for the EES of an eVTOL, describing their characteristics, advantages and disadvantages. Finally, choosing an optimal energy storage solution for the eVTOL, followed with a description of how this system is integrated within the aircraft to deliver the power and energy required.

5.1. Available Theoretical Energy Storage Implementations

5.1.1. Mechanical

Mechanical Energy Storage solutions can be very interesting because they can offer several advantages compared to other EESs, especially in terms of sustainability, environmental impact and cost. The three main types of mechanical energy systems are the flywheel, pumped hydro and compressed air each with different advantages and disadvantages. The main issue is choosing the appropriate system, which depends on several factors like available space, source of the energy and the load.

Flywheel

Flywheel energy storage systems are based on storing energy in the form of kinetic energy by using a certain rotating mass. Most often, it is used for short-term energy storage and in terms of response, they are one of the most effective EESs. Hybrid vehicles, wind power systems, railway, marine and space are all applications where flywheels can be used [15]. Due to their low specific energy, they will not be the optimal energy storage solution for the eVTOL [16].

Pumped Hydro

Next, pumped hydro energy storage is characterized by its low maintenance cost, long cycle life and flexibility. Such a system is formed with three main components namely, an upper reservoir, a pumping system and hydro turbine. The potential gravitational energy of the upper container with respect to the lower one, is what the system relies on. This is, of course, not suitable as energy storage for an aircraft [15].

Compressed Air

The concept of compressed air energy storage is based on storing energy in the form of compressed air. Part of the compressed air will flow trough a natural gas turbine that will produce electricity with a generator, the rest will be used for heating the compressed air, for expansion, before entering the

generator. It is an eco-friendly storage solution with a low maintenance demand [15]. However, the lower energy density due to the weight and size of the required equipment, especially the compressed air tank, makes it far from the best solution for the eVTOL [17].

5.1.2. Electrochemical

Rechargeable Battery

The most popular electrochemical energy storage solution will be the rechargeable battery. Within a battery there are multiple battery cells, each storing electrical energy as chemical energy in two electrodes, an anode and a cathode, which are separated by an electrolyte. This electrolyte will transfer the ionic component of the reaction within the cell and forces the electronic component trough the external circuit outside of the battery [18]. Over the years there have been multiple rechargeable battery technologies developed. Several different combinations of electrolytes and electrode materials are possible, all with different numbers for specific energy, specific power, energy density, power density, safety, performance, life span and costs. One can think of zinc-air, nickel-metal hydride, silver-cadmium, aluminium-ion and, the most used, different kinds of Lithium-ion batteries. To this last group belong, among others, Lithium-ion Manganese Oxide (LMO), Lithium Iron Phosphate (LFP), Lithium Nickel Manganese Cobalt Oxide (NMC), Lithium Nickel Cobalt Aluminium Oxide (NCA) and Lithium-Sulfur (Li-S) [19].

Flow Battery

Another type of an electrochemical battery is the flow battery, a highly efficient energy storage solution. There are two reservoirs for storing charged and discharged electrolytes, a converting system consisting of cells connected in series or parallel, a pump for moving the electrolytes through the converting system and a connection to the load. However, they have a medium to low energy density and require additional parts, as the pump, compared to rechargeable batteries. On top of that, their safety issues contain chemical handling and leakage [20]. All of these points show that a flow battery will not be the optimal energy storage solution for the eVTOL.
As the design contains an eVTOL aircraft, the emphasis is on high specific power and energy, safety and performance when choosing an electrochemical energy storage solution.

5.1.3. Fuel Cell

A fuel cell also converts chemical energy into electricity, but does it different to how a chemical cell does it. Fuel cells can be used with multiple types of fuels, but hydrogen will be considered here as it is the most used. To make a fuel cell storage system work, two components are needed, the fuel tank and the fuel cell. The tank stores the fuel and the cell converts the fuel's energy into electricity. This means that, unlike a chemical cell, such a system cannot have a specific energy and specific power at the same time. Instead, the tank (or the fuel inside) is often rated for energy density and the cell is rated for power density.

[21] compares a fuel cell system to a battery powered system. It states that hydrogen has an energy density of about six times larger than that of batteries. On the other hand, the fuel cell has about a 2.5 times lower power density than the batteries. As the eVTOL will mostly have to be designed around power, it makes more sense to use batteries than to use a hydrogen fuel cell. However, if the eVTOL would have had to fly much further, it would start to make more sense to use a hydrogen fuel cell. Depending on this distance, a hybrid system could be implemented to compensate for the low power from the fuel cell by adding batteries or supercapacitors to the system, as is explained in subsection 5.1.6.

5.1.4. Solid-State

Another way of storing electric energy is through solid state components. They are similar to electrochemical with the workings of multiple cells being able to be connected in series and parallel. However, there are some differences. Several implementations of solid-state batteries are discussed in this section.

Solid-State Batteries

Solid-state cells use a solid electrolyte whereas an electrochemical cell uses a liquid electrolyte. The solid-state battery is a very general term as there are a lot of different solid electrolytes possible for

this application. Its development is rising, but it is still going to take a lot of work to be able to implement this technique into electric vehicles. In the article of [22] it is stated that "In March, the Samsung Advanced Institute of Technology showed the research result of a solid-state battery that can be charged/discharged over 1000 times with 800 kilometers of mileage on a single charge." This is already comparable to and even beats most current standards in EV batteries. Also [23] talks about a battery that is considered the holy grail for battery chemistry because of its high capacity and energy density.

This sounds really promising and would be perfect for this eVTOL, especially as the EIS in 2030 and the first cells might be ready by then. The problem is, however, that currently hardly anyone knows anything about them as development has only just begun. That is why, for the sake of this paper, the choice has been made not to use this type of battery because there is not enough information to base a design upon.

Supercapacitors
Supercapacitors (or ultracapacitors), as stated in [24], have a much higher capacity than regular electrolytic capacitors, discharge faster than electrochemical cells and have a longer cycle life than rechargeable batteries. This would, in theory, make them perfect for aviation, but their main downside is that they have a relatively low energy density. It is so low that almost the entire MTOW of this eVTOL would have to be used to store enough energy. This means that supercapacitors on their own cannot be used as the energy storage system for the eVTOL, but they may be used together with other storage options. This will be discussed in subsection 5.1.6.

Quasi-Solid-State Batteries
In theory, solid-state batteries have more potential for a high power and energy density than current electrochemical cells, but they are much harder to achieve, especially in the short run. Some of the current electrochemical cells can be upgraded, however, by adding solids to their electrolytes. For example, in stead of liquids, the electrolytes are a gel or a paste. These cells result in what are called quasi-solid-state batteries and they can bring along some of the benefits of solid-state batteries to standard electrochemical cells, like mechanical stability. An interesting example is mentioned in [25] where a Lithium Sulfur quasi-solid state cell is pushed to its limits. While mainly focused on cell safety, the article talks about excellent safety against mechanical damage, overheating and short circuit in air or water, but also about performance aspects with a high specific energy, high durability, low self-discharge, and good temperature adaptability. All these aspects show that just tweaking the electrolyte a little bit, can add a lot to the properties of a cell.

5.1.5. Additional Implementations

Magnetic
In the same manner as a supercapacitor uses the theory of capacitance to store electric energy, a superconducting magnetic energy storage (SMES) uses the theory of inductance to store electric energy. However, just like the supercapacitor, it also is not very energy dense. Additionally, SMES systems are less widely used and thus less information can be found on them. [26] has some interesting information on SMES for power grid applications, which shows that they will be much better off on the ground than in the air.

Thermal
Another way of storing electric energy is by storing it as heat. This can be quite energy dense, as is shown in [27], where it is stated to reach 100-500 kWh/m^3, which is comparable to current Li-ion standards. The downside, however, is that this type of storage mostly works well in larger setups, for example in a grid. This is because the setup uses a large turbine with a generator, as is explained in [28]. What this means, is that thermal storage will be too heavy to be used in the eVTOL.

5.1.6. Hybrid Implementations

As was mentioned before, a hybrid implementation where two different energy storage techniques are used can be made as well. This would mainly be done with two storage techniques where one technique has a high power density and the other has a high energy density. This way, they can compensate for each other. For example, a hydrogen setup can be used together with chemical battery cells to achieve

a high energy density, but also be able to put out a lot of power. Comparable to this, a similar setup can be used with chemical battery cells and supercapacitors. With the power and energy that were given in chapter 4 the latter would make the most sense to create. With the battery cell that is chosen in the next section and a hybrid Li-ion supercapacitor from [29] a calculation can be made to see how much a hybrid implementation would benefit the design.

Figure A.10 compares the weight of the battery pack, dependent on the power and energy that has to be delivered. It shows that it barely makes a difference when supercapacitors are added to the design. An interesting addition, however can be seen when the propellers are made smaller, but more are added. Then, the maximum power becomes slightly higher and Figure A.11 shows that a supercapacitor implementation can then decrease the total weight of the energy storage system. According to the Propulsion Team the motors will become more efficient when the propellers become smaller, so it can be a valuable iteration to go over in an upcoming design to change this amount of wings and use a hybrid implementation.

5.2. Battery Pack

5.2.1. Chosen Battery Type

Next, the optimal battery type will be described. For this eVTOL Lithium-Sulfur cells based on the ones from OXIS will be used [30]. Estimations will be made on the available Li-S cells in 2030.
Among the most mature replacements for Li-ion batteries are that of Lithium-Sulfur. The cells replace the metal rich cathode of Lithium-ion cells with comparatively cheap and abundant sulfur. Lithium-Sulfur presents a number of advantages in comparison with other, currently available, battery technologies. They have an improved specific energy density, improved safety characteristics, reduced material costs and a reduced environmental burden associated with the used materials [31]. All these main four advantages will now be individually further explained.

The most important and significant advantage of Lithium-Sulfur batteries is the substantially higher energy density that can be achieved. Li-S cells have a theoretical specific energy of 2700 Wh/kg. While this number will be reduced when the technology is deployed in a cell, functional prototypes of 450 Wh/kg have already been produced [32]. OXIS has provided a plan for the coming years and stated that targets have been set at 600 Wh/kg and 900 Wh/L, to be achieved by 2026 [32]. These specifications will be used to estimate a Li-S battery cell for use in 2030 (eVTOL EIS) as this provides a 4-year buffer to cover any unforeseeable setbacks and other developments.

The operating mechanism of Li-S batteries offer significant safety advantages over other types. The reactive Lithium anode is passivated with a sulfide material, this reduces the risk of dangerous failure of the battery. While thermal runaway still exists in these cells, research has shown that the magnitude of this failure is significantly lower compared to Li-ion batteries [31]. A Li-S pouch cell battery is even able to withstand nail penetration without any significant effects [33]. Next to the fact that Lithium-Sulfur is still a technology in development, OXIS already powered an all-electric aircraft back in 2020, meeting FAA requirements [32]. Proving that the technology is already suitable for aviation use.

The largest part of battery costs are from metals including nickel and cobalt. The materials used in the electrodes of Li-S cells are comparatively of lower cost, with sulfur being amongst the most present element on earth in contrast to other materials used. This can result in Li-S batteries with lower prices and improved performance compared to Li-ion systems. Removing metals like cobalt is an important consideration too due to ethical and environmental concerns with mining and uncertainties around supplies [31].

As mentioned earlier, Li-ion batteries consist of both cobalt and nickel which are gained trough intensive mining efforts. As battery technology is used more widely around the globe, the impact of fabricating these cells is becoming more of an increasing concern. Also, the supply of these metals is finite. In contrast, the sulfur used in Li-S batteries is so abundant that it it described as 'almost limitless' by the US Geographical Survey. Next, sulfur is available across all continents and has no major health risks connected to it [31].

Next to the technological advantages of a technology or technique, an engineer should also think about aspects like ethics and the environment which can be easily overlooked. Additionally, Lithium-Sulfur has been chosen as the energy storage solution for the eVTOL as it would be a more original choice compared to currently available more safe options like standard Lithium-ion batteries. This is considered a positive byproduct as 25% of all points can be scored with originality in the IEEE Challenge described within chapter 1.

These specific cells have been used before on an aircraft [32] and the development within OXIS is looking promising. In 2019 OXIS introduced two different Lithium-Sulfur cells, one high energy cell and one high power cell. Their specifications are stated in Table 5.1

Table 5.1: 2019 OXIS Li-S Cells and Assumed 2030 Li-S Cell Specifications

Specification	**Higher Energy Cell (OXIS 2019)**	**High Power Cell (OXIS 2019)**	**Assumed Cell (2030)**
Nominal Voltage [V]	2.1	2.1	2.3
Nominal Energy [Ah]	14.7	19	33
C-Rating [-]	2	6	7
Cell Weight [g]	85	141	150

This table first of all shows the two cells from OXIS with their specifications. It also shows an assumed cell, because the EIS for the eVTOL would be in 2030 and by then Li-S cells will have developed a lot compared to current Li-S cells. OXIS has made the statement that in 2026 their cells will have an energy density of 600 Wh/kg. When taking the average of the energy density of the current cells and comparing this to the statement from OXIS, an assumption could be made that their cell in 2030 could very well have a nominal energy of 33 Ah. This assumption will be used for the design of the energy storage, but a margin of ±20% will also be used for the nominal energy because this assumption can end up being either too low or too high. On top of the assumption based on OXIS' statement, the other specifications need to be adjusted slightly to keep up with development. This is why the nominal voltage has been increased slightly to get it more into the middle between the lowest and highest voltage. Also, the maximum power has been increased slightly and the cell weight has been rounded up. This would give an estimated pack weight of 190 kilograms (160-240 kilograms at ±20% Ah), but this is yet without packaging and a BMS with cooling and also not taking into account the voltages and currents that need to be delivered to the motors.

5.2.2. Battery Pack Layout

With the assumed cell and the knowledge of the maximum power and needed energy, the battery pack can be designed. First of all the voltage and current output of the pack has to be defined. This is defined by the voltage that the inverters for the motors use which will be 800 V. Using 800 V on a 900 kW system, means that 1125 A is needed to power the entire system. Using these two values a 350s4p pack would be needed, meaning that there are 350 cells in series and 4 cells in parallel. DC/DC boost converters are used to help the battery pack put out a constant voltage. This means that the battery pack will create a slightly lower voltage and a higher current than needed and the DC/DC converters will convert this directly when it is coming out of the pack. With this system, a bit less cells have to be placed in series as more can be placed in parallel. The DC/DC converter can then make sure that the output voltage is always steady at 800V, independent of the cell voltages which will change with the SOC. Additionally, there will also be a DC/DC buck converter which transforms power to 12V for all auxiliary devices in, for example, the control system and cooling system.

To help with redundancy and to prevent voltage drops when the battery is low on charge, it is best to split up the big battery pack into several smaller modules which add up to a voltage that would be higher than the needed voltage so the DC/DC converter can always regulate the voltage to be 800 V at the output. For these two requirements to work, several packs would need to be placed in series and these combinations would then also need to be placed in parallel, so when one pack fails, the other parallel combination(s) can still deliver power.

Keeping this division in mind, the values in Table 5.2 could be derived, also for packs with a ±20% margin. The amount of series cells and the amount of parallel modules have been kept the same for all the packs for simplicity. The amount of parallel cells is adjusted slightly to keep the maximum output current approximately the same for the three different packs. The amount of series modules is calculated using the lowest value for the cell voltage (1.9 V) and making sure that the entire pack has a high enough maximum power together with the other calculated amounts. The values for the pack voltage, current, weight and energy are calculated using the values from Table 5.1. As can be seen, the maximum power and total energy inside the pack stays approximately the same for all the packs, but mainly the weight differs between the packs. This deviation is approximately 25% which is slightly higher than the margin, because the capacity in Ah also influences the maximum output power because of the constant C-Rating.

Table 5.2: Specifications for Li-S Battery Pack together with ±20% margin

Specification	Assumed Cell	+20% Ah	-20% Ah
Nominal Cell Energy [Ah]	33	26.4	39.6
Module Parallel Cells	3	3	4
Module Series Cells	24	24	24
Parallel Modules	2	2	2
Series Modules	13	11	13
Pack Nominal Voltage [V]	717	607	717
Pack Peak Current [A]	1386	1663	1478
Pack Peak Power [kW]	995	1010	1061
Pack Weight [kg]	281	238	374
Pack Energy [kWh]	142	144	156

DC/DC Converters from [34] were used which are capable of handling 50-1000 A. This is of course not enough to transform the maximum current, which is why two of them will be used; one for every wing. The power from the battery pack can be transformed directly at the output of the pack, so the high current does not have to be conducted through the wires. This minimizes losses due to heat created by high currents and thus thinner wires can be used throughout the eVTOL to minimize weight as well. These DC/DC converters would have an efficiency of 98 to 99% and weigh approximately 2.5 kilograms each. This outcome does mean that the eVTOL is taking along more kWh than necessary, but this is needed to accommodate for the maximum power that the eVTOL uses. What this means, is that the eVTOL will have a projected range of approximately 160 kilometers.

The battery pack alone will not suffice, however, as there will also have to be packaging around it, a BMS needs to be included with cooling and the pack will need cabling. The BMS will be explained later on, but right now an estimation on the weight of all these components can already be made. This estimation will be done by comparing current standards. A Tesla battery module (a car drives on ±16 of these modules) weighs 26.3 kilograms [35] and contains 444 Panasonic 18650 cells which weigh 48.5 grams each [36]. This means that 21.5 kg of the module is made up of battery cells. Conclusively, it can be said that approximately 20% of a battery modules is used for packaging, a BMS with a cooling system and cabling of a module. For the entire pack, an additional 5% is added to account for the additional cabling and attachments. This means that the battery pack would eventually weigh approximately 351 kilograms ±25%, depending on the capacity of the cells.

6

Charging

The current problem of charging EVs is the time needed in comparison with refueling a non-electric vehicle. If EV or eVTOL charging wants to compete with petroleum-based (air) transportation, battery charging times need to come down significantly. Energy storage and charging of EVs is comparable to that of eVTOLs, as they are both reliant on batteries and use electric motors to move forward. State-of-the-Art and prospective charging methods for EVs will be evaluated and applied to the eVTOL. As electric vehicles are currently becoming more and more popular advances are also made in the field of charging [37].

6.1. State-of-the-Art

Charging of electrochemical batteries has come a long way over the past decade. At a certain point, Direct Current Fast Charging (DCFC) Level 1 was reached with a average power delivery of 1.4 kW. Moving forward to Level 3, an average power of 50 kW was reached. Currently, there are multiple EV Charging standards on the market with various maximum output powers. Some available standards are CHAdeMO 2.0 with a maximum power of 400 kW, GB/T with a maximum power of 185 kW, CCS2 with a maximum power of 350 kW and Tesla Specific with a maximum power of 140 kW [38]. To this day, the Combined Charging System 2 (CCS2), which is DCFC Level 5, is the fastest commercially available charging method at up to 350 kW power output, this is with a maximum voltage of 900 V and current of 400 A [37] [38].

6.2. Future Perspective

The current rise of the electric vehicle calls for a new, fast, safe and global DC charging standard. Nicknamed ChaoJi, a new DC charging method combined two of the most used international DC fast charging system, namely CB/T and CHAdeMO. ChaoJi started as a Japan-China bilateral project back in 2018 and has come a long way since then. The unprecedented work led to the creation of a brand-new plug that is able to handle 900 kW, while ensuring safety and backwards compatibility with existing charging standards. It has currently evolved to an international technical collaboration platform of experts beyond the two countries. The initial targeted specs were to deliver 900 kW at 1500 V and 600 A, which could be increased to 1800 kW with additional voltage pins. The defined characteristics are a simple, compact and light connector, liquid-cooled cable to be able to handle 600 amperes and Vehicle-to-Everything (V2X) ready. Protocol and certification tests have been completed in the first quarter of 2021 and ChaoJi is ready to become globally available in the coming few years [38]. It seems the obvious choice to use ChaoJi for the charging of the eVTOL as it will be commercially available in the coming years, compatible with other standards and can currently handle the most power in comparison to other standards.

6.3. eVTOL Charging

As Li-S is the chosen electrochemical energy storage solution for the eVTOL, its charging capabilities have to be investigated. The 2019 OXIS Li-S Cell described earlier in this chapter, has a maximum charge rate of 0.25C stated by the datasheet [30]. This is, however, without any modifications to the cell or active cooling of the cell. Next-generation Li-S energy storage devices face a few challenges including the ability of fast-charging. To be able to increase the charge rates, the stability of the electrodes should be improved with an efficient electrochemical system. Research has shown that only a small modification is needed to create a highly stable long-term cycling performance Li-S battery [39].

Fast charge and discharge rates cause a faster decrease in lifetime and capacity of batteries, this is however not the case with the use of another binder. Testing showed a minor capacity decay after 500 cycles of 0.026% at 5C and 0.029% at 10C. This approach has the potential to significantly improve the design of the next-generation Li-S energy storage solution [39]. The high charge rate of Li-S batteries is also confirmed by [40]. Further research on Li-S fast charging is expected over the coming years, resulting in a commercially available solution in 2030 for use in the eVTOL. With this information in mind, the upcoming ChaoJi standard would be able to fully charge the eVTOL with the mentioned 142 kWh Li-S battery pack in an estimated 14 minutes (11-17 min. with ±20%). This can be seen in Figure 6.1. These minutes could be effectively used to unload and load the cargo of the eVTOL.

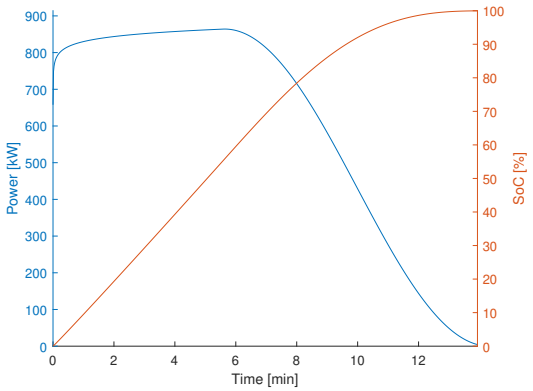

Figure 6.1: Charge Power & SoC v Time (ChaoJi 900 kW)

The charge voltage of a Li-S is on average higher than the discharge voltage, which can be seen in [41]. The used 2030 Li-S cell has an estimated nominal discharge voltage of 2.3 V, consequently the charge voltage is set on 2.5 V. As the battery has an discharge voltage of 715 V, estimated is a charge voltage of 775 V. ChaoJi has a maximum power of 900 kW, so the maximum current has been set at 1115 A resulting in a maximum power of 890 kW. The batteries will be charged at peak at a C-rating of around 6, this section has shown the feasibility of this rate. Not the whole capacity of a battery can be charged at this maximum rate due to physical limitations, Figure A.12 shows the variable current and voltage over time including the CC/CV transition point. As the exact voltage curve of current Li-S cells and the estimated used 2030 cell is not known, estimated is that the charge power will start dropping at around 50% SOC, resulting in Figure 6.1.

As mentioned earlier in section 6.2, the ChaoJi has the potential to increase it maximum power to 1800 kW with additional pins. If this upgrade would be commercially available in 2030, the EIS of the eVTOL and the Li-S cells would be able to handle the current, the battery could be fully charged within an estimated 7.5 minutes (6-9 minutes with ±20%), this can be seen in Figure A.14. A maximum charge current of 2300 A, 12.5 C, would be used, resulting in a maximum charge power of 1780 kW which will start dropping at a lower SOC compared to the mentioned 890 kW due to the higher power. For all the mentioned graphs, they are simplified and based on estimations and assumptions for the 2030 Li-S cell. Their purpose is to give an estimate of the time required to charge the eVTOL battery.

How the charger will be implemented in the eVTOL can be seen in Figure A.8, a block diagram shows how the charge current and voltage are controlled via the BMS according to battery pack measurements. The DC/DC converter is needed to convert the ChaoJi maximum power of 1500 V/600 A to the maximum 775 V/1150 A used for charging the battery. Additionally, the 142 kWh battery of the eVTOL can be used to feed power back to the electrical grid using the Vehicle-to-Everything (V2X) protocol. This can be for personal use, or when the prices or the demand is high. The eVTOL can then be recharged when the prices and demand are low. This feature could have a great potential in 2030 because each coming year, the electrical grid will be used more heavily [42].

7

Battery Management System

There exist many applications where batteries are the primary, and often the only, solution for the storage of electric energy. One can think of uninterruptible power supplies (UPS), renewable energy systems, cordless electric power tools, electric vehicles and, of course, eVTOLs [43]. The performance of a battery when connected to a load or a source is based on a number of chemical reactions inside the battery. These chemicals degrade with usage and time which results in the gradual reduction in the electrochemical storage capacity of the battery. Preferably this depreciation process needs to be kept to a minimum, this is done by controlling its discharging and charging profile in a suitable way. This holds for various load conditions but especially heavy loads. Generally, the life time of the battery will diminish when the battery is operated under frequent discharge and charge cycles and a wide range of thermal conditions. Particularly high-pulse current conditions will harm the battery life. In general, batteries are safe, apart from some reports of failure or explosion when used correctly with an added system that incorporates the safety feature and integrated automatic shutdown [44]. However, thanks to two main key mechanisms, the use of a ceramic lithium sulfide passivation layer and a non-flammable electrolyte, Lithium-Sulfur batteries can withstand extreme conditions. A Li-S cell will show no adverse reaction to a bullet or nail penetration in contrast to a Li-ion cell [33].
For an eVTOL, battery monitoring is vital because the safety and operation depends on the battery system. The latter is exactly the major function of a Battery Management System (BMS). It is there to control and check the status of the battery within its specified operating conditions. A BMS consists of multiple modules with different tasks to optimize the usage and life of the battery system. This chapter will describe the different aspects of the BMS integrated in the eVTOL. A complete block diagram with all the different modules of the BMS used in the eVTOL can be found in Figure A.9. This diagram will make it easier to understand how all of the concepts are implemented and interconnected.

7.1. Monitoring

The function of the Measurement Block will be to measure the individual cell voltages, total battery current and the temperature at different points within the battery pack. All these values will be converted to digital values to later be used to estimate the battery status in later stages of the BMS. The reason that all cell voltages will be measured individually, despite the additional hardware needed, is that in this case balancing and overcharge protection at cell level is possible.

7.2. Control and Protection

7.2.1. Equalization

There can be minor variations within capacity, internal resistance and discharge and charge characteristic between batteries. To maximize the battery's capacity and lifetime, cell balancing is a very important BMS function. The Equalization Block will compare the differences between all the battery cells. If there is a difference detected greater than the predefined threshold, the balancing process is initiated. Usually, the highest voltage cell is discharged trough a discharge resistor until the difference in voltage is diminished [44]. This method will be used. However, Lithium-Sulfur Battery Packs have

a specific characteristic. Li-S Cells have a self-balancing feature, this is due to the self-discharge that takes place at higher levels of SOC. Approximately above the 70% SOC mark, at the Li-S high voltage plateau, this discharging is the most significant. The indicated self-discharging during operation, of in series connected cells, will result in SOC equalization due to the energy dissipation during self-discharge. This self-discharging can however be converted to so called self-balancing. This is done via adjustments in temperature conditions, charging limits and time spent at higher SOC, so at the high voltage plateau. These changes will lead to an influence on the self-balancing rate [45]. Further research into the self-balancing characteristic of Lithium-Sulfur is expected to be done over the coming years. Following from this will be controlled self-balancing of the Lithium-Sulfur Battery Pack within the eVTOL in 2030.

7.2.2. Thermal Management

The Thermal Management Block will monitor and control the temperature of the battery pack, according to the incoming temperature measurements from sensors within the battery pack. It prevents the battery from being harmed by very high, or very low, temperatures and tries to keep the battery back at the optimal operating temperature. The optimal temperature for the used Lithium-Sulfur cell in 2030 is yet to be determined in further research in the years to come. The Thermal Block will read the ambient and battery pack temperatures and initiates, if needed, heating or cooling operations. One can imagine that heating is needed before take-off to pre-heat the battery pack to the optimal operating temperature. Cooling will be needed when the battery is discharged at higher C-ratings due to internal resistances and (thermal) losses which increases the temperature of the pack.
To control the temperature of the battery a cooling liquid will flow in between the cells, touching the sides of the battery cells to exchange heat. The way the liquid will flow trough the cells can be seen in Figure 7.1. Assumptions concerning thermals include that natural convection transfers heat from the cell to the surrounding fluid gap between the cells, as mentioned. On top of that, a recirculating loop trough the battery pack will carry the heated fluid from the bottom cells of the back to the top where it then flows down the sides of the eVTOL, which has a cooler ambient temperature, where it exchanges heat. Next, the the cooled liquid can enter the bottom of the battery pack again. Especially during flight at high velocity, the liquid can be cooled significantly with the cool ambient air. When stationary or charging, the liquid will be actively cooled next to exchanges heat with the ambient environment [46].

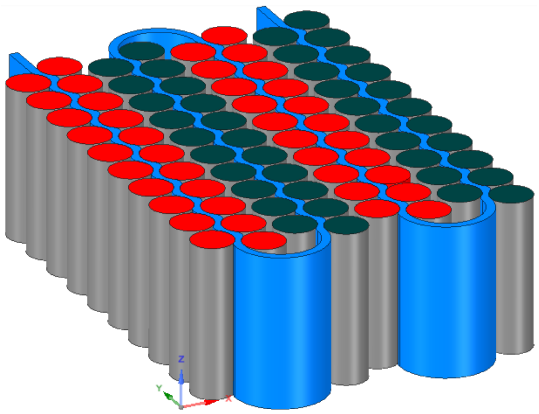

Figure 7.1: Liquid Cooling Flow trough Battery Pack. Adapted from [46]

7.3. Estimation

7.3.1. State-of-Charge Estimation

Over the course of history, different methods have been developed to estimate the State-of-Charge (SOC) of electrochemical batteries. One method more suitable for certain battery technologies than the other. The most widespread conventional method is the so-called *Coulomb Counting*. Also used to benchmark other techniques. In this concept, the SOC is estimated by integrating the current from the load. From this current the used and remaining capacity of the battery can be estimated. Assuming SOC_0 as the initial SOC at the time t_0, the SOC of the battery cell at time t is calculated by the following equation:

$$SOC = SOC_0 - \left(\int_{t_0}^{t} \frac{\gamma \, i(\tau)}{C_t} d\tau \right), \quad 0 < SOC < 1 \tag{7.1}$$

Where $i(t)$ is the current and assumed negative for charging and positive for discharging. Next, γ is the coulombic efficiency of the cell and C_t is the total capacity. Following this method, the value of the SOC will be between 0 and 1, with 0 representing a fully depleted state and 1 a fully charged state. However, *Coulomb Counting* suffers from accumulated errors due to initial SOC value errors, measurement errors and noise. Also, C_t can change under various (temperature) condition which can result to errors in the SOC estimation when using this method [47]. The SOC estimation of Li-S batteries is not directly comparable to that of most Li-ion cells. This is mainly due to Li-S flat cell voltage curve compared to that of the SOC. An example of a flat Lithium-Sulfur voltage curve can be seen in Figure 7.2.

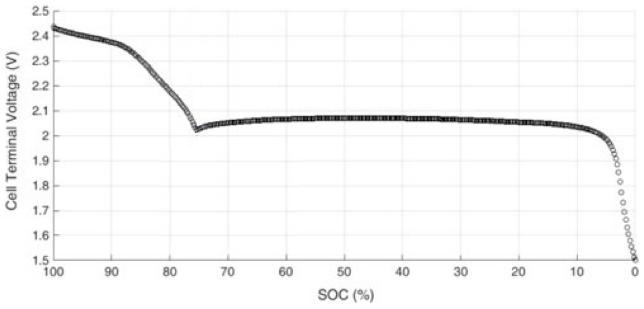

Figure 7.2: Li-S Cell Terminal Voltage during discharge at C/30. Adapted from [47]

The method that will be used to estimate the SOC of the Li-S battery pack within the eVTOL is a new technique, developed by [48]. The new method includes a hybrid of two estimation methods. First, an equivalent-circuit-network (ECN) model is parameterized using the data obtained from the Li-S cell. For this estimating technique, the Thevenin model will be used. The approach of ECN modelling is chosen for its effectiveness in both computational speed and accuracy. The model consists of the open circuit voltage of the battery (U_{OC}), an ohmic resistor (R_0) (thermal losses), a polarization resistor (R_P) and a polarization capacitor (C_P). How exactly this parameters will be calculated and how it can be applied for the whole battery pack can be found in [48]. Next, a Forgetting Factor Recursive Least Square (FFRLS) identification algorithm is used. The reason for this is that for application in eVTOLs or EVs, it is preferred to have a quick and simple algorithm suitable for real time application. The algorithm is used to identify parameters of a discrete model with four unknown parameters. These are U_{OC}, R_0, R_P and C_P which will be formulated in vector θ parameters. Thereafter, the parameters will be fed to a Support Vector Machine (SVM) classifier to estimate the SOC range in the form of a cluster number between 1 and 10. Eventually, the results are combined with Coulomb Counting to give continuous estimates. This is necessary because the SVM SOC classifier generates a discrete cluster, in this case a number between 1 and 10 is generated. So, it is only known if the SOC is between 10% and 20% or 70% and 80%, for example. The SVM alone is not enough to provide a smooth continuous SOC estimating. Using such a hybrid system, including a SVM Classifier and Coulomb Counting, not only a continuous estimation is achieved but additional SOC accuracy is gained. How both the SVM and Coulomb Counting are combined, is shown in the following equation:

$$SOC_H = \frac{W1 \cdot SOC_{SVM} + W2 \cdot SOC_{CC}}{W1 + W2} \tag{7.2}$$

Where SOC_H is the hybrid estimated SOC, SOC_{SVM} is the SOC provided by the SVM and SOC_{CC} is the SOC from the Coulomb Counting. $W1$ and $W2$ are the fusion gains. There are given to the estimated values of the SVM and Coulomb Counting, respectively. This way, the balance between both estimators can be shifted. The main advantage of the SVM is that a better guess of the initial condition provided. When making $W1$ larger than $W2$, the SVM is prioritized which leads to a quicker convergence. Nonetheless, it fluctuates more around the reference SOC after the convergence. Vice versa, when $W1 < W2$ the convergence will be slower however, it leads to a value very close to the reference SOC after the convergence. A solution to optimize for both parts to gain a more accurate SOC estimation is to implement adaptive gains. So, start by prioritizing SOC_{SVM} and slowly move the emphasis

towards SOC_{CC} as the battery discharges. Testing shows that the best performance regarding SOC is achieved when $W1 = 0.9$ and $W2 = 0.1$ at the beginning of estimation and change to $W1 = 0.1$ and $W2 = 0.9$ after convergence. All due to the remarkable voltage curve of Li-S [48]. In Figure A.9 can be seen how this SOC estimation is implemented within the BMS. Also, it explains how the different modules of the SOC estimation work together to provide the final estimations and it makes it easier to understand the overall implementation and layout of the BMS with all of its modules.
According to the results shown by [48] the hybrid system is able to estimate the Li-S cell's State-of-Charge with a maximum error of 2.63% and a average error of >1% from any initial condition. The Lithium-Sulfur cell used for all the testing by [48] is the OXIS Energy Ultra Light Li-S Pouch Cell, the same cell as mentioned in section 5.2. There is expected more research will be done concerning this method over the coming years. Especially, more in-depth testing should be done regarding the effect of cell ageing. Because the parameters of the model will be influenced by aging an additional modification factor should be added to the SOC estimator to compensate for this consequence. An improved SOC estimating method is expected to be commercially ready in 2030, the EIS of the eVTOL.

7.3.2. State-of-Health Estimation

The State-of-Health (SOH) is defined as the percentage of the nominal capacity that is still left in the battery. Discharge and charge cycles and aging are the major factors that worsen the SOH of a battery [49]. The SOH is estimated using the measured battery parameters such as the temperature, current and voltage of the battery. For a Lithium-Sulfur battery the SOH can be estimated with combinations of single parameters that will be fed to a SVM classifier to estimate the SOH using multiple parameters. The paper from [49] explains in detail how exactly this Li-S SOH estimating works. Results show that using this method, the SOH can be estimated with a level of accuracy of 96.7%. Another important discovery done on Lithium-Sulfur battery cells is that the loss of power output over time is much lower than the loss of capacity, this is a useful feature for powering an eVTOL as a high maximum power is needed for take-off [49]. There is expected that the mentioned SOH estimation method is matured by 2030 and it is ready to be used within the eVTOL. Again, how the State-of-Health estimation module is implemented within the BMS can be seen in Figure A.9.

7.3.3. Capability Estimation

Once an accurate estimation has been done for the SOC and SOH of the battery pack, the BMS has to determine the maximum discharge and charge current at any given time of operation. The function of the Capability Estimation Block within the BMS is to provide information about safe levels of charging and discharging current of the battery to the charger and Control Systems. This is very important information as it prevents the battery from being charged or discharged beyond the specified limitations and guarantees safe operations. The BMS can restrict the current according to a function that depends on the SOC, SOH, voltage and temperature of the cells [44]. Also, an emergency signal is sent to Control Systems if an abnormal rise in temperature is detected to immediately take action. Figure A.9 show the implementation of the Estimation Block and all of its inputs and outputs. Control Systems will use the information received from the BMS to check if the battery shows acceptable values at all times and all operations can continue accordingly.

8

Conclusion and Future Work

8.1. Conclusion

In the end an eVTOL and its energy storage system has successfully been designed with the information necessary to participate in the **AIAA/IEEE challenge** as stated in chapter 1.

- The eVTOL design considerations have settled on a design with two fixed wings, attached to the fuselage at an angle and at different heights on the body. Both wings each have four propellers connected perpendicular to the wing via their own motors. The size of the propellers has been designed to minimize the maximum power needed to take off vertically. The fuselage is designed to be able to transport most cargo up to 1000 kilograms.
- The electric propulsion system design has partly been created in this thesis, going over specifically the energy storage with corresponding voltages and currents and additional specifications.
- The concepts of operation have been determined partly in this thesis, settling on only cargo transport and mentioning the energy refill strategy.

The way the eVTOL has been designed, is according to the program of requirements as mentioned in chapter 2. The eVTOL has a range of 100 kilometers with a 25 kilometer backup at a cruise speed of 250 km/h. Its operating range is 150 meters from the ground and can take off with a maximum weight of 2500 kilograms. The aircraft also fits within a 15-meter diameter circle while on the ground and airborne. The entire design is able to be implemented by 2030 and will produce zero CO_2 at its vehicle level. An overview of all the specifications can be found in Table 3.1. The requirements for the **eVTOL design** have been fulfilled with the following specifications;

- The wings have a wingspan of 11.5 meters and a wing chord of 0.87 meters, giving them a wing aspect ratio of 13.2 and a taper ratio of 1. With the lift coefficient of 0.42 this makes them able to lift 2500 kilograms at a cruise speed of 250 km/h,
- There is a total of eight propellers connected to the eVTOL. They each have a radius of 1.5 meters, making them able to accelerate the eVTOL with a total take-off weight of 2500 kilograms at 3 m/s^2,
- The fuselage has a droplet-like shape as seen from the front and has the dimensions of 5 meters depth by 0.75 meters wide and high, giving a total volume of around 3 m^3 of which approximately two thirds can be used for cargo. This leaves enough room to carry 1000 kilograms which is about the largest possible payload with the MTOW of 2500 kilograms,
- The entire design is aerodynamic and has adequate lift and drag coefficients as was possible to be achieved in the given time span.

The requirements for the **Energy Storage System** have been fulfilled with the following specifications;

- The energy storage system consists of a Lithium-Sulfur battery pack,
- The energy storage system can create a maximum power of 995 kW which is enough for the eVTOL to accelerate the total take-off weight of 2500 kilograms vertically at 3 m/s^2,
- The energy storage system can store 142 kWh which is enough to fly approximately 160 kilometers, which is more than the required 100 + 25 kilometers,

- The nominal voltage of the energy storage is 717 V and this is regulated by DC/DC converters to give a constant 800 V output to the inverters which is the right voltage for the motors to achieve their required RPM,
- The maximum current of the energy storage is 1386 A which is the right current for the motors to achieve their required maximum torque,
- The energy storage system has a Battery Management System with monitoring and managing functions to equalize the voltages in the battery cells and keep the temperatures in a safe range. It also has SOC, SOH and capability estimation,
- The charging system uses a ChaoJi standard that can charge up to 900 kW. It will be used to charge at 890 kW which will charge the system in approximately 14 minutes from 0 to 100% SOC. It will charge at a maximum of 775 V with 1115 A, both depending on the SOC.

8.2. Future Work

The results of this thesis seem promising. However, some aspects are still coupled with assumptions and estimations. There is expected that this will improve when accurate information will become available over the coming years. Currently, a relatively accurate estimation for the 2030 eVTOL can be done as some of the techniques already seem applicable up to a certain extent. To reach to goal of a fully operation eVTOL according to the requirements provided several tasks still need to be completed within the coming years.

Further research, as described earlier in the thesis or as there is an information gap, must be done containing;

- The amount of propellers to optimize motor torque, as discussed in subsection 3.2.1,
- An iteration of the structural and aerodynamic efficiency of the fuselage and wing design to optimize aerodynamics, as discussed in subsection 3.4.1,
- The efficiency of Lithium-Sulfur battery packs to improve optimization, as discussed in subsection 4.4.1,
- The energy storage hybrid solution with a Lithium battery plus supercapacitors to improve weight to power ratio, as discussed in subsection 5.1.6,
- The developments of Lithium-Sulfur batteries in the current decade, especially power and energy characteristics, as discussed in subsection 5.2.1,
- The developments of the ChaoJi and other upcoming charging standards to improve the charging aspects, as discussed in section 6.2,
- The potential of the V2X capability of eVTOLs in 2030, as discussed in section 6.3,
- The fast charging capabilities of Lithium-Sulfur batteries to improve optimization, as discussed in section 6.3,
- The self-balancing characteristic of Lithium-Sulfur batteries to improve the lifetime of the battery, as discussed in subsection 7.2.1,
- The optimal operation temperature of Lithium-Sulfur batteries during different states of discharging and charging to improve optimization, as discussed in subsection 7.2.2,
- The (hybrid) State-of-Charge estimation of Lithium-Sulfur batteries to improve the estimation accuracy, as discussed in subsection 7.3.1,
- The State-of-Health estimation of Lithium-Sulfur batteries to improve the estimation accuracy, as discussed in subsection 7.3.2.

If all of the above will be completed before the EIS of the eVTOL, there will in all probability be a fully operational commercially available eVTOL aircraft with a maximum payload and no CO_2 emission by the vehicle in 2030.

A

Graphics

A.1. eVTOL Renders

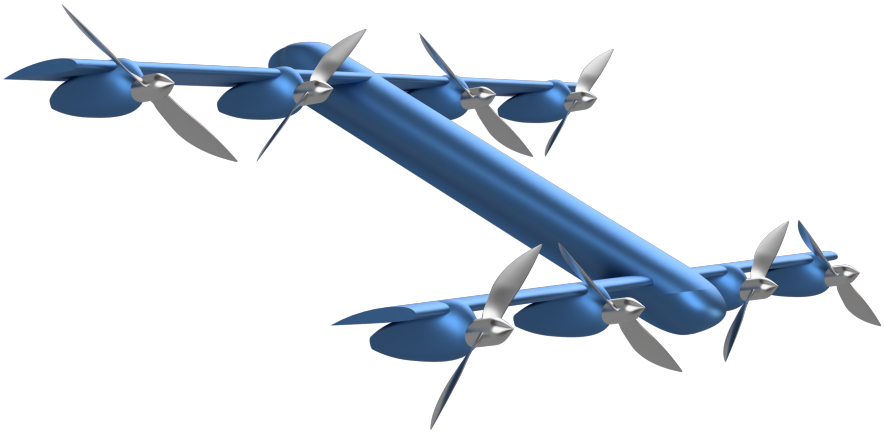

Figure A.1: Render of the eVTOL during Cruise

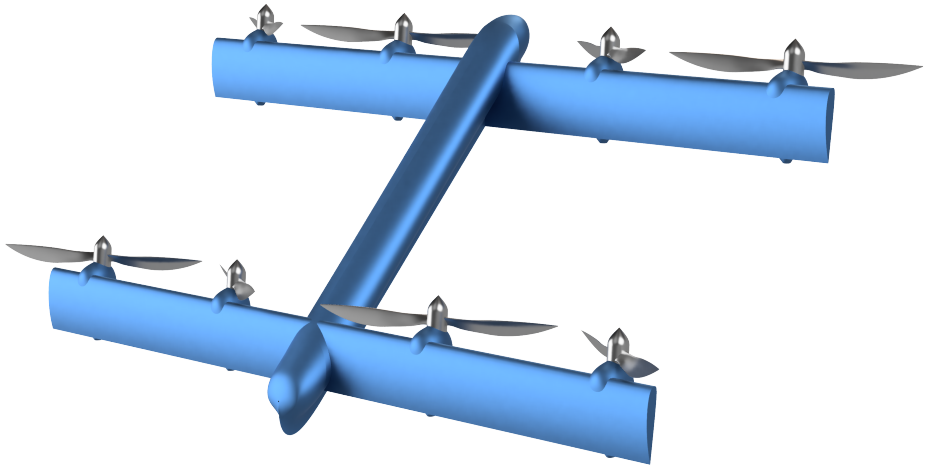

Figure A.2: Render of the eVTOL during Take-Off

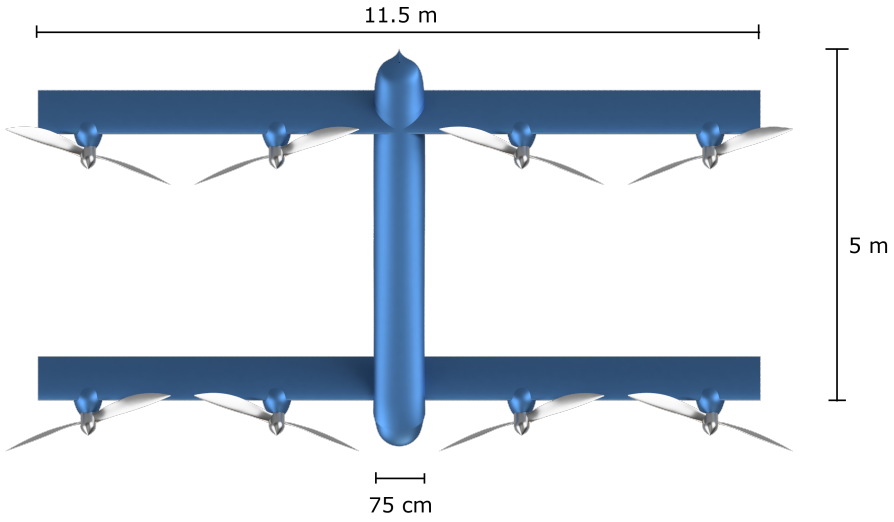

Figure A.3: Render of the eVTOL from the Top including dimensions

Figure A.4: Render of the eVTOL from the Side

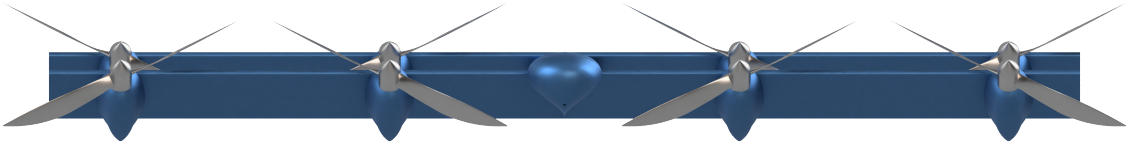

Figure A.5: Render of the eVTOL from the Front

A.2. Schematics

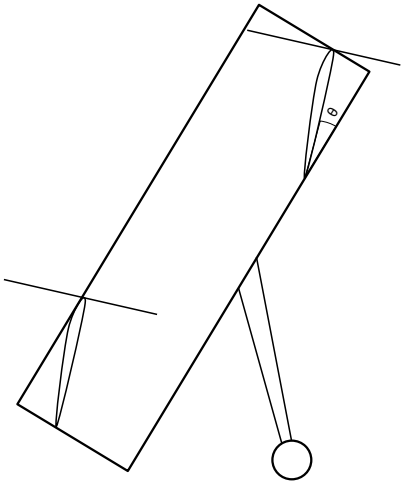

Figure A.6: Schematic of the eVTOL as seen from the Side with Landing Gear

A.3. Block Diagrams

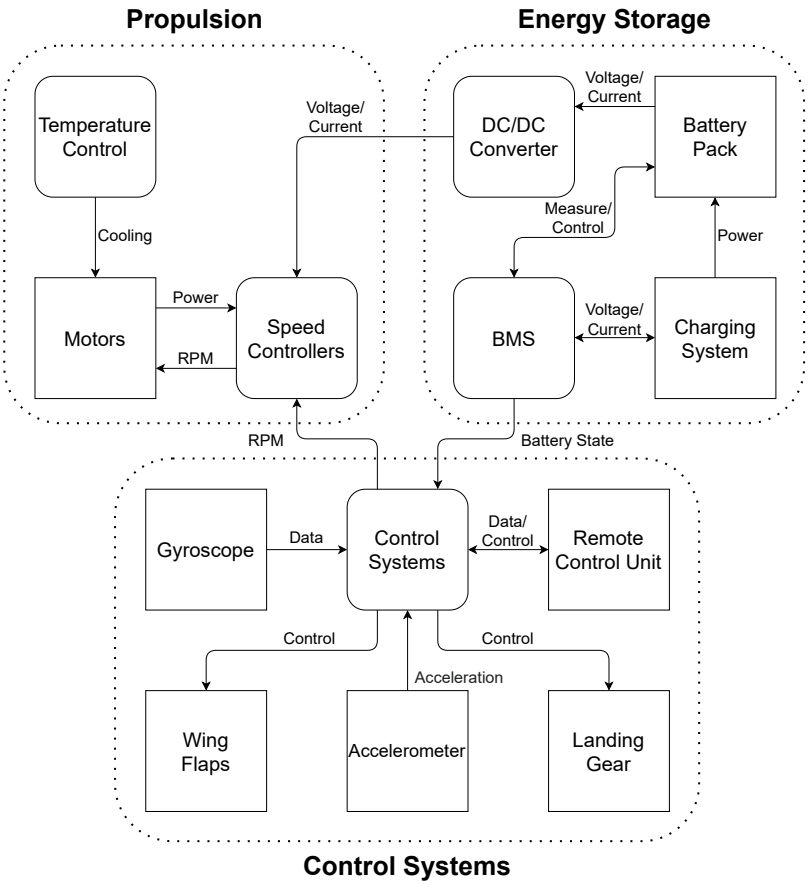

Figure A.7: Subgroup Division and Electrical Design Block Diagram

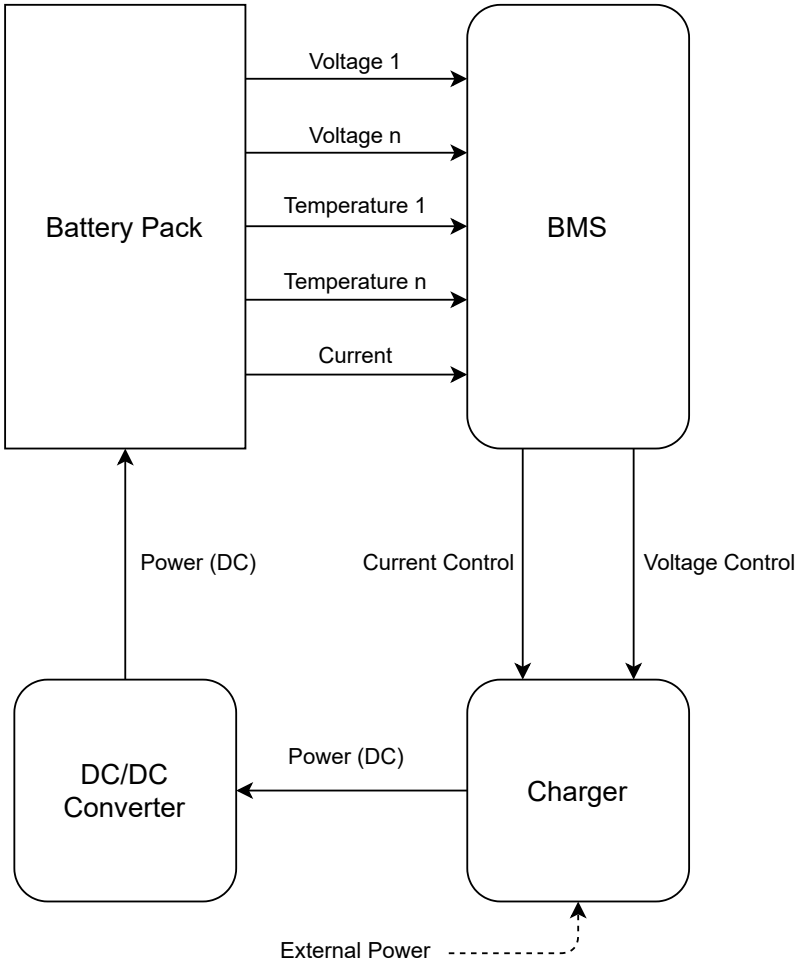

Figure A.8: Charging Solution Block Diagram

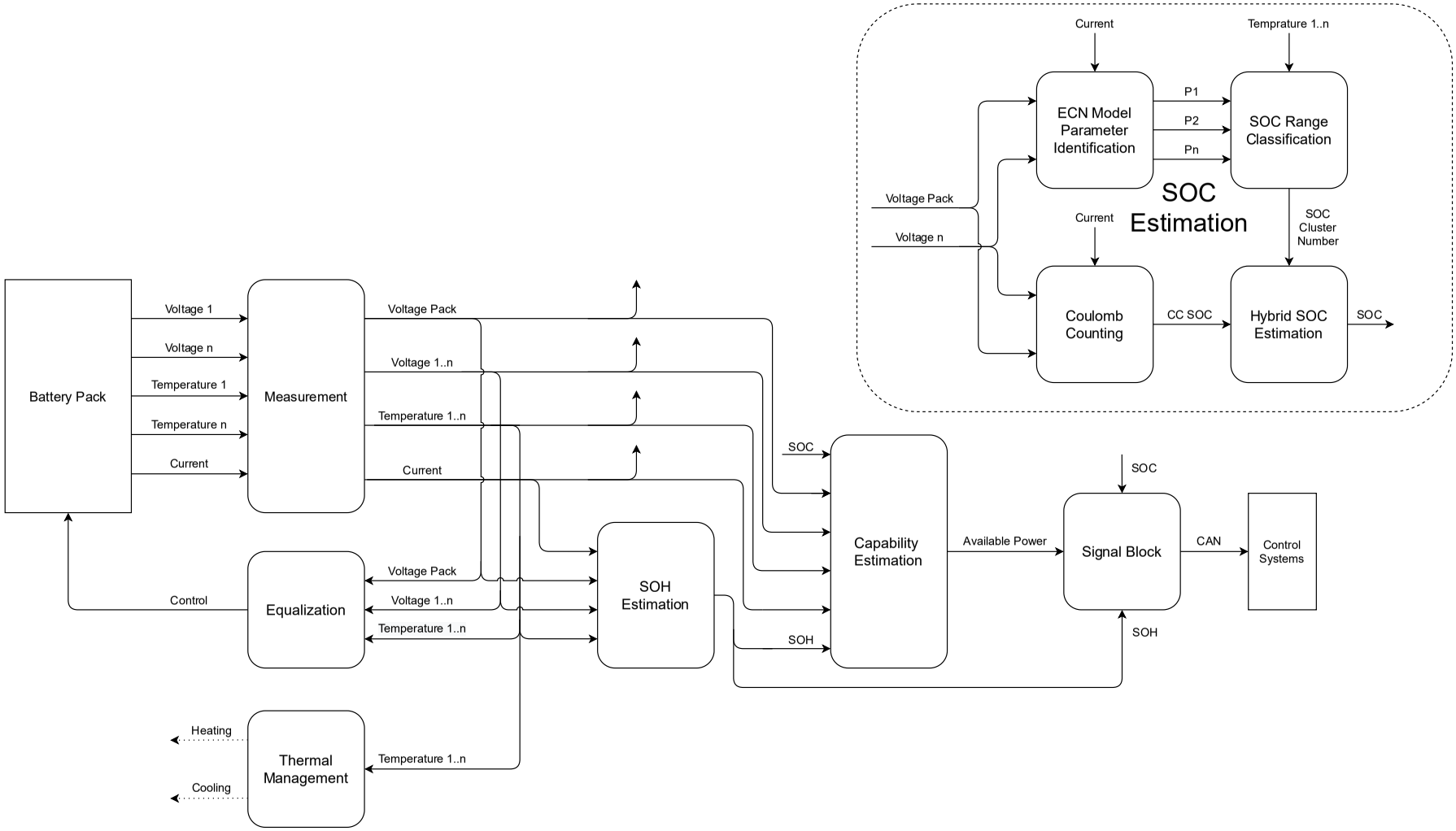

Figure A.9: Battery Management System Block Diagram

A.4. Plots

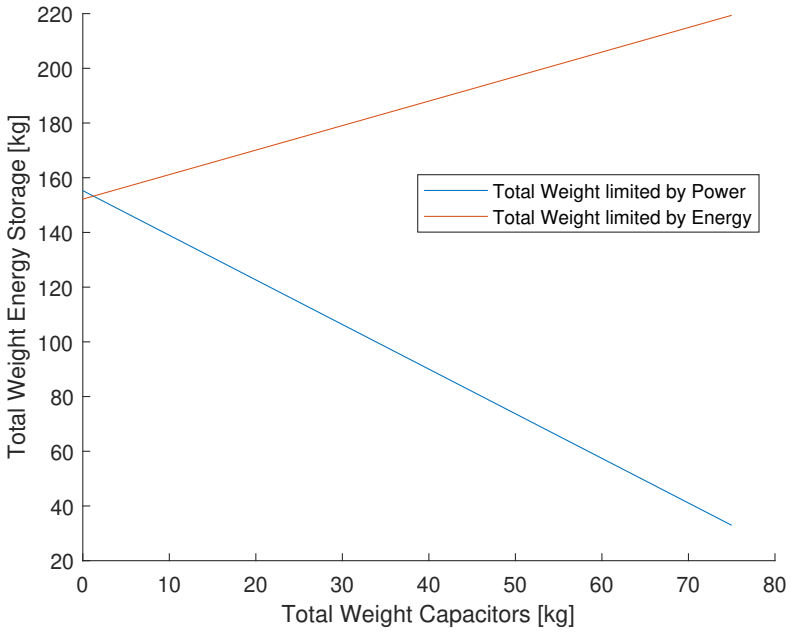

Figure A.10: Hybrid Storage Implementation with Power and Energy for Design from chapter 4

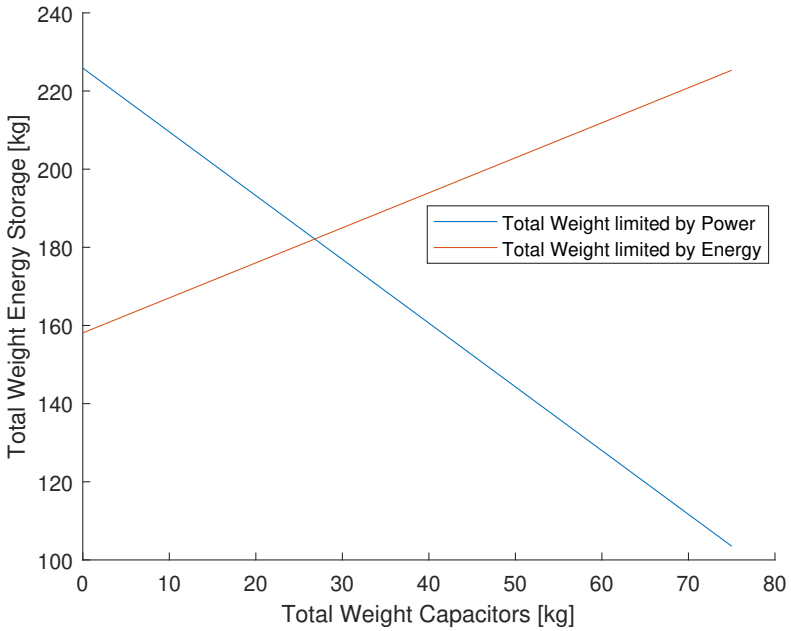

Figure A.11: Hybrid Storage Implementation with Power and Energy for Design with Smaller and More Propellers

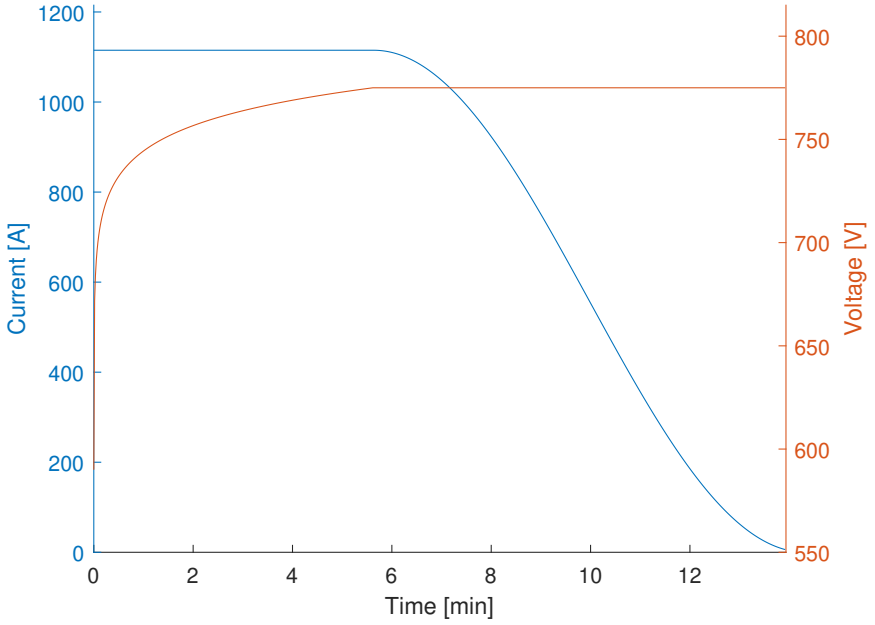

Figure A.12: Charge Voltage & Current v Time (ChaoJi 900 kW)

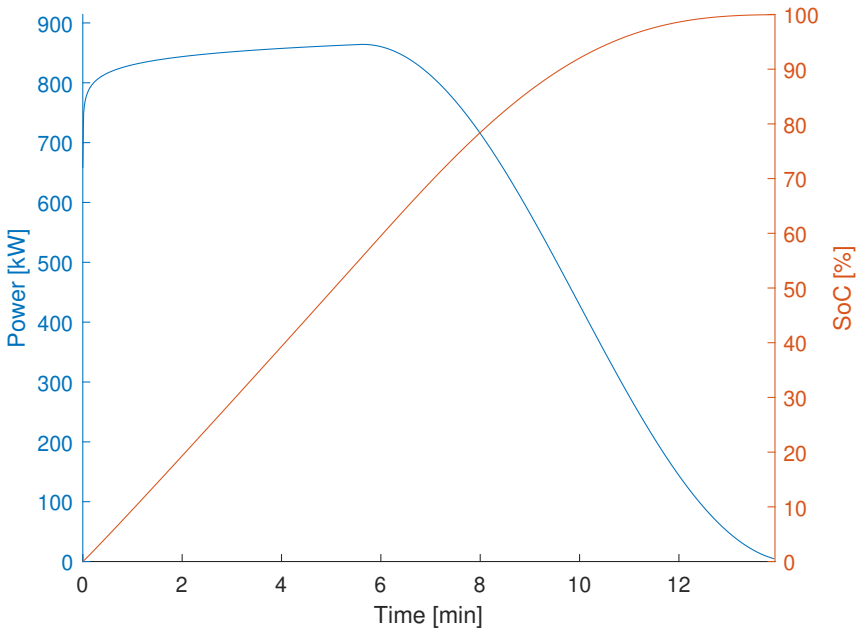

Figure A.13: Charge Power & SoC (%) v Time (ChaoJi 900 kW)

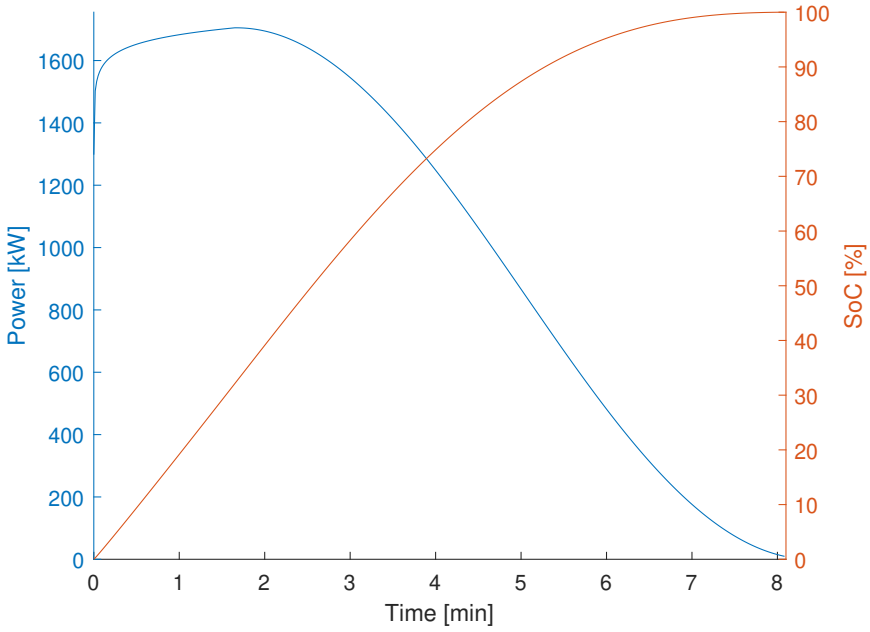

Figure A.14: Charge Power & SoC (%) v Time (ChaoJi 1800 kW)

B

Matlab Code

B.1. Aircraft Calculation

B.1.1. Aerodynamic Design Specifications

```
clear variables;

%% Some Initial Values which can be played with
chord_ratio = repmat(0.15, 1, 10);
fuselage_width = repmat(1.5, 1, 10);
fuselage_length = repmat(5, 1, 10);
wing_area = repmat(20, 1, 10);
% fuselage_drag = [1.2, 1.2, 1.2, 1.2, 1.2, 1.2, 1.2, 1.2, 1.2, 1.2];  %
 ↪  This is the drag coefficient of a circle in 2D
fuselage_drag = repmat(0.1, 1, 10);

% R = repmat(1.5, 1, 10);
% theta = repmat(60, 1, 10);

%% Plot Radius to Power and Radius to Energy (Uncomment entire section to
 ↪  plot)
R = [1.15, 1.2, 1.25, 1.3, 1.35, 1.4, 1.45, 1.5, 1.55, 1.6];
theta = [45, 45, 45, 45, 45, 45, 45, 45, 45, 45];
[wing_span, wing_chord, wing_distance_max, C_l, C_d, C_d0,
 ↪  Thrust_Horizontal, Thrust_Vertical, Thrust_Laying_to_Vertical,
 ↪  Thrust_Vertical_Landing_1, Thrust_Vertical_Landing_2,
 ↪  Power_Horizontal, Power_Vertical, Power_Laying_to_Vertical,
 ↪  Power_Landing_1, Power_Landing_2, Energy_Horizontal, Energy_Vertical,
 ↪  Energy_Landing, Total_Energy, Drag_Zero_Lift_Fuselage] = forloop(R,
 ↪  chord_ratio, theta, fuselage_width, fuselage_length, wing_area,
 ↪  fuselage_drag, 0);
hold on;
yyaxis left
xlim([1.15, 1.6]);
ylim([750, 1150]);
% title("Comparison of different Propeller Radii with the Peak Power and
 ↪  Energy Demand");
plot(R, Power_Laying_to_Vertical/1000);
xlabel("Radius [m]");
ylabel("Maximum Power [kW]");
```

```
yyaxis right
plot(R, Total_Energy/1000);
ylabel("Total Energy [kWh]");

%% Plot Total Energy and Maximum Power (Uncomment entire section to plot)
R = [1.5, 1.5, 1.5, 1.5, 1.5, 1.5, 1.5, 1.5, 1.5, 1.5];
theta = [5, 10, 15, 20, 25, 30, 35, 40, 45, 50];
[wing_span, wing_chord, wing_distance_max, C_l, C_d, C_d0,
 ↪ Thrust_Horizontal, Thrust_Vertical, Thrust_Laying_to_Vertical,
 ↪ Thrust_Vertical_Landing_1, Thrust_Vertical_Landing_2,
 ↪ Power_Horizontal, Power_Vertical, Power_Laying_to_Vertical,
 ↪ Power_Landing_1, Power_Landing_2, Energy_Horizontal, Energy_Vertical,
 ↪ Energy_Landing, Total_Energy, Drag_Zero_Lift_Fuselage] = forloop(R,
 ↪ chord_ratio, theta, fuselage_width, fuselage_length, wing_area,
 ↪ fuselage_drag, 0);
hold on;
yyaxis left
% title("Comparison of different Wing/Body Angles with the Peak Power and
 ↪ Energy Demand");
plot(theta, Power_Laying_to_Vertical/1000);
xlabel("Angle of Wing against Body [deg]");
ylabel("Maximum Power [kW]");

yyaxis right
plot(theta, Total_Energy/1000);
ylabel("Total Energy [kWh]");

%% Plot Power / Energy Ratio with legs underneath (Uncomment entire
 ↪ section to plot)
R = [1.5, 1.5, 1.5, 1.5, 1.5, 1.5, 1.5, 1.5, 1.5, 1.5];
theta = [27.5, 30, 32.5, 35, 37.5, 40, 42.5, 45, 47.5, 50];
leg_length = [1, 3, 4, 4.5, 5];
x=10;
Power_Laying_to_Vertical = zeros(length(leg_length),x);
Total_Energy = zeros(length(leg_length),x);
for i = 1:1:length(leg_length)
    [wing_span, wing_chord, wing_distance_max, C_l, C_d, C_d0,
     ↪ Thrust_Horizontal, Thrust_Vertical, Thrust_Laying_to_Vertical,
     ↪ Thrust_Vertical_Landing_1, Thrust_Vertical_Landing_2,
     ↪ Power_Horizontal, Power_Vertical, Power_Laying_to_Vertical(i,:),
     ↪ Power_Landing_1, Power_Landing_2, Energy_Horizontal,
     ↪ Energy_Vertical, Energy_Landing, Total_Energy(i,:),
     ↪ Drag_Zero_Lift_Fuselage] = forloop(R, chord_ratio, theta,
     ↪ fuselage_width, fuselage_length, wing_area, fuselage_drag,
     ↪ leg_length(i));
end

hold on;
yyaxis left
xlim([27.5, 50]);
% title("Comparison of different Wing/Body Angles with the Peak Power to
 ↪ Energy Demand Ratio with Legs");
for i = 1:1:length(leg_length)
    plot(theta, Power_Laying_to_Vertical(i,:)/1000);
end
```

```
xlabel("Angle of Wing to Body [deg]");
ylabel("Ratio of maximum Power to Energy demand [kW]");

yyaxis right
plot(theta, Total_Energy(1,:)/1000);
ylabel("Energy Demand [kWh]");
legend("Nose Height from Ground = 1", "Nose Height from Ground = 3", "Nose
 ↳ Height from Ground = 4", "Nose Height from Ground = 4.5", "Nose Height
 ↳ from Ground = 5", "Energy Demand");

%% Plot Power / Energy Ratio at Vertical Acceleration (Uncomment entire
 ↳ section to plot)
R = [1.5, 1.5, 1.5, 1.5, 1.5, 1.5, 1.5, 1.5, 1.5, 1.5];
theta = [40, 42.5, 45, 47.5, 50, 52.5, 55, 57.5, 60, 62.5];
[wing_span, wing_chord, wing_distance_max, C_l, C_d, C_d0,
 ↳ Thrust_Horizontal, Thrust_Vertical, Thrust_Laying_to_Vertical,
 ↳ Thrust_Vertical_Landing_1, Thrust_Vertical_Landing_2,
 ↳ Power_Horizontal, Power_Vertical, Power_Laying_to_Vertical,
 ↳ Power_Landing_1, Power_Landing_2, Energy_Horizontal, Energy_Vertical,
 ↳ Energy_Landing, Total_Energy, Drag_Zero_Lift_Fuselage] = forloop(R,
 ↳ chord_ratio, theta, fuselage_width, fuselage_length, wing_area,
 ↳ fuselage_drag, 0);
hold on;
yyaxis left
xlim([40, 62.5]);
title("Comparison of different Wing/Body Angles with the Peak Power to
 ↳ Energy Demand Ratio");
plot(theta, Power_Vertical./Total_Energy);
xlabel("Angle of Wing to Body [deg]");
ylabel("Ratio of maximum Power to Energy demand [W/Wh] (C Rating)");

yyaxis right
plot(theta, Total_Energy/1000);
ylabel("Energy Demand [kWh]");

%% Additional Plot
R = repmat(0.75, 1, 10);
theta = repmat(37, 1, 10);
[wing_span, wing_chord, wing_distance_max, C_l, C_d, C_d0,
 ↳ Thrust_Horizontal, Thrust_Vertical, Thrust_Laying_to_Vertical,
 ↳ Thrust_Vertical_Landing_1, Thrust_Vertical_Landing_2,
 ↳ Power_Horizontal, Power_Vertical, Power_Laying_to_Vertical,
 ↳ Power_Landing_1, Power_Landing_2, Energy_Horizontal, Energy_Vertical,
 ↳ Energy_Landing, Total_Energy, Drag_Zero_Lift_Fuselage] = forloop(R,
 ↳ chord_ratio, theta, fuselage_width, fuselage_length, wing_area,
 ↳ fuselage_drag, 0);
hold on;
yyaxis left
xlim([40, 85]);
title("Comparison of different Wing/Body Angles with the Peak Power and
 ↳ Energy Demand");
plot(theta, Power_Laying_to_Vertical/1000);
xlabel("Angle of Wing against Body [deg]");
ylabel("Maximum Power [kW]");
```

```
yyaxis right
plot(fuselage_length, Total_Energy/1000);
ylabel("Total Energy [kWh]");

%% For Loop
function [wing_span, wing_chord, wing_distance_max, C_l, C_d, C_d0,
 ↪  Thrust_Horizontal, Thrust_Vertical, Thrust_Laying_to_Vertical,
 ↪  Thrust_Vertical_Landing_1, Thrust_Vertical_Landing_2,
 ↪  Power_Horizontal, Power_Vertical, Power_Laying_to_Vertical,
 ↪  Power_Vertical_Landing_1, Power_Vertical_Landing_2,
 ↪  Energy_Horizontal, Energy_Vertical, Energy_Landing, Total_Energy,
 ↪  Drag_Zero_Lift_Fuselage] = forloop(R, chord_ratio, theta,
 ↪  fuselage_width, fuselage_length, wing_area, fuselage_drag, leg_length)
    x = 10;  % Change this number to the amount of tests to be done

    props = 8;  % We are using 8 propellors to help redundancy and torque
     ↪  of motors
    m = 2500;  % Mass of entire aircraft equals 2500kg
    rho = 1.225;  % Air Density
    v_cruise = 69.5;  % Cruise Speed
    acc = 3;  % Vertical Acceleration

    % Necessary for Matlab purposes
    wing_span = zeros(1,x);
    wing_chord = zeros(1,x);
    wing_distance_max = zeros(1,x);
    C_l = zeros(1,x);
    C_d = zeros(1,x);
    C_d0 = zeros(1,x);
    Thrust_Horizontal = zeros(1,x);
    Thrust_Vertical = zeros(1,x);
    Thrust_Laying_to_Vertical = zeros(1,x);
    Thrust_Vertical_Landing_1 = zeros(1,x);
    Thrust_Vertical_Landing_2 = zeros(1,x);
    Power_Horizontal = zeros(1,x);
    Power_Vertical = zeros(1,x);
    Power_Laying_to_Vertical = zeros(1,x);
    Power_Vertical_Landing_1 = zeros(1,x);
    Power_Vertical_Landing_2 = zeros(1,x);
    Energy_Horizontal = zeros(1,x);
    Energy_Vertical = zeros(1,x);
    Energy_Landing = zeros(1,x);
    Total_Energy = zeros(1,x);
    Drag_Zero_Lift_Fuselage = zeros(1,x);

    % The for loop
    for i = 1:1:x
        A_temp = pi * R(i)^2;
        theta_temp = theta(i);
        chord_ratio_temp = chord_ratio(i);
        fuselage_width_temp = fuselage_width(i);
        fuselage_length_temp = fuselage_length(i);
        fuselage_drag_temp = fuselage_drag(i);
        wing_area_temp = wing_area(i);
```

```
        [wing_span(i), wing_chord(i), wing_distance_max(i),
         ↪ Thrust_Horizontal(i), Power_Horizontal(i),
         ↪ Drag_Zero_Lift_Fuselage(i), C_l(i), C_d(i), C_d0(i)] =
         ↪ horizontal_cruise(props, rho, v_cruise, chord_ratio_temp,
         ↪ theta_temp, A_temp, fuselage_width_temp,
         ↪ fuselage_length_temp, fuselage_drag_temp, wing_area_temp);
        [Thrust_Vertical(i), Power_Vertical(i)] =
         ↪ vertical_acceleration(wing_span(i), wing_chord(i), rho,
         ↪ C_d(i), m, acc, A_temp, props);
        [Thrust_Laying_to_Vertical(i), Power_Laying_to_Vertical(i)] =
         ↪ laying_to_vertical(theta_temp, props, A_temp, rho,
         ↪ Thrust_Vertical(i), leg_length, fuselage_length_temp);
        [Thrust_Vertical_Landing_1(i), Thrust_Vertical_Landing_2(i),
         ↪ Power_Vertical_Landing_1(i), Power_Vertical_Landing_2(i)] =
         ↪ vertical_deceleration(m, acc, props, A_temp, rho);
        [Energy_Vertical(i), Energy_Horizontal(i), Energy_Landing(i),
         ↪ Total_Energy(i)] = total_energy(Power_Vertical(i),
         ↪ Power_Horizontal(i), Power_Vertical_Landing_1(i),
         ↪ Power_Vertical_Landing_2(i));
    end
end

%% Horizontal Cruise Function
function [wing_span, wing_chord, wing_distance_max, Thrust_Horizontal,
 ↪ Power_Horizontal, Drag_Zero_Lift_Fuselage, C_l, C_d, C_d0] =
 ↪ horizontal_cruise(props, rho, v_cruise, chord_ratio, theta, A,
 ↪ fuselage_width, fuselage_length, fuselage_drag, wing_area)
    wing_span = sqrt(wing_area /(chord_ratio));  % The wing span is a
 ↪ function of the wing area
    wing_chord = wing_area / (2 * wing_span);  % The wing chord is a
     ↪ function of the wing area and wing span

    C_l = 2 * 25000 / (wing_area * rho * v_cruise^2);  % We calculated the
     ↪ lift coefficient accordingly

    wing_distance_max = 2 * sqrt(7.5^2 -
     ↪ ((wing_span+fuselage_width)/2)^2);  % This would be the maximum
     ↪ distance between the wings
    fuselage_frontal_area = fuselage_width * fuselage_length *
     ↪ sin(deg2rad(theta));  % Calculate the frontal area of the fuselage
     ↪ according to the wing angle
    Drag_Zero_Lift_Fuselage = lift_and_drag(fuselage_drag,
     ↪ fuselage_frontal_area, rho, v_cruise);  % The fuselage is assumed
     ↪ to be some cylinder at an angle

    AR = wing_span^2/wing_area;
    e = 1.78*(1-0.045*AR^0.68)-0.64;
    C_d = 1/(pi*e*AR)*C_l^2;  % The drag coefficient is calculated
     ↪ according to the lift coefficient and some assumed values for the
     ↪ wing area and wing span
    Drag_Induced = lift_and_drag(C_d, wing_area, rho, v_cruise);  %
     ↪ Induced drag

    mu = 1.81e-5;
    Re = rho * v_cruise * wing_chord / mu;
```

```
    Cf = 1.327 / sqrt(Re);
    tc = 0.2;  % Assumption
    ftc = 1 + 2.7 * tc + 100 * tc^4;
    M = v_cruise / 343;
    fm = 1 - 0.08*M^1.45;
    Swet = 2; S = 1;  % Assumption
    C_d0 = Cf * ftc * fm * Swet / S * (C_d / 0.004)^0.4;
    Drag_Zero_Lift_Wing = lift_and_drag(C_d0, wing_area, rho, v_cruise);
     ↪ % Zero Lift Wing Drag. Is approximately a third of the induced
     ↪ wing drag

    Thrust_Horizontal = (Drag_Zero_Lift_Wing + Drag_Zero_Lift_Fuselage) /
     ↪ 0.6 + Drag_Induced;  % Calculated zero lift drag is approximately
     ↪ 60% of the total zero lift drag

%     Power_Horizontal = props * sqrt((Thrust_Horizontal / props)^3 / (2 *
 ↪ A * rho));
    Power_Horizontal = Thrust_Horizontal * v_cruise;
end

%% Vertical Acceleration
function [Thrust_Vertical, Power_Vertical] =
 ↪ vertical_acceleration(wing_span, wing_chord, rho, C_d, m, acc, A,
 ↪ props)
    F_acc = m * (10 + acc);  % Accelerating Force
    T = F_acc:1:F_acc+5000;
    A_wing = wing_span*wing_chord/2;
    v_vert = back_velocity(T, rho, A);  % Back velocity of one propeller
     ↪ in vertical acceleration
    F_drag = lift_and_drag(C_d, A_wing, rho, v_vert);  % Drag force
    F_vert = T - props*F_drag;
    acceleration = F_vert / m;

    % plot(T, acceleration);

    Thrust_Vertical = T(find(acceleration>10+acc, 1));  % As long as the
     ↪ thrust is high enough to reach the acceleration, this thrust is
     ↪ used

    Power_Vertical = props * sqrt((Thrust_Vertical / props)^3 / (2 * A *
     ↪ rho));
end

%% Laying to Vertical Operation
function [Thrust_Laying_to_Vertical, Power_Laying_to_Vertical] =
 ↪ laying_to_vertical(theta, props, A, rho, Thrust_Vertical, leg_length,
 ↪ fuselage_length)
    angle = deg2rad(theta + asind(leg_length / fuselage_length));  % This
 ↪ angle is the wing angle against the body plus a potential landing gear
 ↪ angle
    Thrust_Laying_to_Vertical = Thrust_Vertical / sin(angle);
    Power_Laying_to_Vertical = props * sqrt((Thrust_Laying_to_Vertical /
     ↪ props)^3 / (2 * A * rho));
end
```

```
%% Vertical Deceleration
function [Thrust_Vertical_Landing_1, Thrust_Vertical_Landing_2,
 ↪  Power_Vertical_Landing_1, Power_Vertical_Landing_2] =
 ↪  vertical_deceleration(m, acc, props, A, rho)
    Thrust_Vertical_Landing_1 = m * (10 - acc);  % Some very global
 ↪  estimations for landing power
    Thrust_Vertical_Landing_2 = m * (10 - acc/2);

    Power_Vertical_Landing_1 = props * sqrt((Thrust_Vertical_Landing_1 /
     ↪  props)^3 / (2 * A * rho));
    Power_Vertical_Landing_2 = props * sqrt((Thrust_Vertical_Landing_2 /
     ↪  props)^3 / (2 * A * rho));
end

%% Energy Needed for Entire Flight
function [Energy_Vertical, Energy_Horizontal, Energy_Landing,
 ↪  Total_Energy] = total_energy(Power_Vertical, Power_Horizontal,
 ↪  Power_Vertical_Landing_1, Power_Vertical_Landing_2)
    Energy_Vertical = Power_Vertical * 1.5/60;  % Wh  @ 1.5 minutes
    Energy_Horizontal = Power_Horizontal * 30/60;  % Wh  @ 30 minutes
    Energy_Landing_1 = Power_Vertical_Landing_1 * 0.75/60;  % Wh
    Energy_Landing_2 = Power_Vertical_Landing_2 * 0.75/60;  % Wh
    Energy_Landing = Energy_Landing_1 + Energy_Landing_2;  % Wh  @ 1.5
     ↪  minutes for total landing

    Total_Energy = Energy_Vertical + Energy_Horizontal + Energy_Landing_1
     ↪  + Energy_Landing_2;
end

%% Functions
function v = back_velocity(T, rho, A)
    v = sqrt(T ./ (2 * A * rho));
end

function F = lift_and_drag(C, A, rho, v)
    F = C * A * rho * v.^2 / 2;
end
```

B.1.2. Wing to Body Angle

```
clear variables;

fuselage_length = 5;
fuselage_width = 0.75;
chord_length = 0.87;
prop_radius = 1.5;

theta = 0:0.1:90;

prop_area = pi * prop_radius ^ 2;
wing_d = fuselage_length - chord_length .* cos(deg2rad(theta));

% 1
```

```
dy1 = wing_d .* sin(deg2rad(theta));
dyRp1 = dy1 ./ prop_radius;

% 2
dd = fuselage_width - chord_length * sin(deg2rad(theta));
x = sqrt(dd.^2 + wing_d.^2);
phi = (90 - rad2deg(atan(wing_d/dd))) + theta;
dy2 = x .* sin(deg2rad(phi));
dyRp2 = dy2 ./ prop_radius;
angle_min = theta(find(dyRp2>2, 1));

hold on;
plot(theta, dyRp1);
plot(theta, dyRp2);
yline(2);
legend("Wings at same Height", "Front Wing Lower", "dy/Rp = 2");
xlabel("Wing to Body Angle [deg]");
ylabel("Lateral Distance between Propellers dy/Rp");

final_theta = 37;
a = fuselage_width / 2 - chord_length * sin(deg2rad(final_theta)) / 2;
b = fuselage_length / 2 - chord_length * cos(deg2rad(final_theta)) / 2;
angle_to_ground = rad2deg(atan(a/b)) + 37;
```

B.2. Capacity Calculation

B.2.1. Power and Energy Consumption

```
clear variables;

%% You can change all this
vertical_altitude = 75;
cruise_altitude = 150;
landing_altitude = 75;
cruise_velocity = 250/3.6;

props = 8;
R = 1.5;

distance = 125;  % km

a_vertical = 3;
a_transition = 3;
a_retransition = 2;
a_landing = -2;

t_start = 5;
% t_horizontal = 30*60;
t_end = 5;

%% And then this will be calculated accordingly
t_vertical = sqrt(vertical_altitude./a_vertical);
t_horizontal = 1000 * distance / cruise_velocity;
```

```
t_transition = cruise_velocity/a_transition;
t_retransition = cruise_velocity/a_retransition;
t_landing_1 = sqrt((cruise_altitude-landing_altitude)./-a_landing);
t_during_landing = 1;
t_landing_2 = landing_altitude/(-t_landing_1*a_landing);

Energy_Vertical = vertical_energy(a_vertical, t_vertical, props, R);
Energy_Horizontal = horizontal_energy(1.39e5, t_horizontal);
Energy_Landing_1 = vertical_energy(a_landing, t_landing_1, props, R);
Energy_Landing_2 = vertical_energy(-a_landing, t_landing_2, props, R);
Energy_Transition = linear_energy(t_transition, Energy_Vertical(1),
 ↪  Energy_Horizontal(1));
Energy_Retransition = linear_energy(t_retransition, Energy_Horizontal(1),
 ↪  Energy_Landing_1(1));
Energy_During_Landing = linear_energy(t_during_landing,
 ↪  Energy_Landing_1(1), Energy_Landing_2(1));
Energy_Start = linear_energy(t_start, 0, Energy_Vertical(1));
Energy_End = linear_energy(t_end, Energy_Landing_2(1), 0);

dt_hor = 60;
Energy_Total = cat(2, Energy_Start, Energy_Vertical, Energy_Transition,
 ↪  Energy_Horizontal(1:dt_hor*10), Energy_Retransition,
 ↪  Energy_Landing_1, Energy_Landing_2, Energy_End);

Total_Energy = sum([Energy_Start, Energy_Vertical, Energy_Transition,
 ↪  Energy_Horizontal, Energy_Retransition, Energy_Landing_1,
 ↪  Energy_Landing_2, Energy_End])/36000;

%% And eventually you get a nice little plot
total_t = t_start + t_vertical + t_transition + 60 + t_retransition +
 ↪  t_landing_1 + t_landing_2 + t_end;
min = (length(Energy_Total)-600) / total_t * 100;
dt_min = (length([Energy_Start, Energy_Vertical, Energy_Transition,
 ↪  Energy_Horizontal])/10 - dt_hor)/60;
first_min = (length([Energy_Start, Energy_Vertical,
 ↪  Energy_Transition])/10+dt_hor)/60;

plot(Energy_Total/1000);
xticks([0, 0.5*min, (first_min)*min, (first_min+0.5)*min]);
xticklabels({'t = 0', 't = 30 s', ['t = ' num2str(ceil(dt_min)) ' min'],
 ↪  ['t = ' num2str(ceil(dt_min)) ' min & 30s']});
ylabel(”Power [kW]”);
text(min, 500, ['Total Energy Used \approx ',
 ↪  num2str(ceil(Total_Energy/1000)), 'kWh']);

%% Weird Stuff because Matlab can't just break axes
axes('Position',[0.425 0.08 0.05 0.05]);
px=[1 5];
py1=[1 2];
height=1;
py2=py1+height;
plot(py1,px,'k','LineWidth',2);hold all;
plot(py2,px,'k','LineWidth',2);hold all;
fill([py1 flip(py2)], [px flip(px)],'w','EdgeColor','none');
box off;
```

```
axis off;

%% Functions
function Energy_Vertical = vertical_energy(a, t, props, R)
    m = 2500;
    A_wing = 20;
    rho = 1.225;
    A = pi*R^2;
    C_d = 0.0137;

    F_acc = m * (10 + a);
    T = F_acc:1:F_acc+10000;
    v_vert = sqrt(T ./ (2 * A * rho));
    F_drag = C_d * A_wing * rho * v_vert.^2 / 2;
    F_vert = T - 4*F_drag;
    acceleration = F_vert / m;
    Thrust = T(find(acceleration>10+a, 1));
    Power_Vertical = props * sqrt((Thrust / props)^3 / (2 * A * rho));
    Energy_Vertical = repmat(Power_Vertical, 1, floor(t*10));
end

function Energy_Linear = linear_energy(t, P_start, P_end)
    time = 0:1:floor(t*10);
    Energy_Linear = (P_end-P_start)/(10*t) .* time + P_start;
end

function Energy_Horizontal = horizontal_energy(P, t)
    Energy_Horizontal = repmat(P, 1, floor(t*10));
end
```

B.2.2. Hybrid Storage

```
clear variables;

power_max = 800e3;  % W
% power_hor = 1.39e5;  % W
energy_tot = 80e3;  % Wh
% energy_vert_tot = power_vert*30/3600;  % Wh

power_cap = 9320;
energy_cap = 52.56;
power_li_s = 2.3*33*7*1000/150;  % Peak power; cannot withstand for entire
 ↪ flight
energy_li_s = 2.3*33*1000/150;

capacitors_grams = 0:1000:75000;
li_ion_grams_power = zeros(1,length(capacitors_grams));
li_ion_grams_energy = zeros(1,length(capacitors_grams));
for i = 1:1:length(capacitors_grams)
    total_power_cap = capacitors_grams(1,i) * power_cap / 1000;
    needed_power_from_li_ion = power_max - total_power_cap;
    li_ion_grams_power(i) = needed_power_from_li_ion / power_li_s * 1000;
```

```
    total_energy_cap = capacitors_grams(1,i) * energy_cap / 1000;
    needed_energy_from_li_ion = energy_tot - total_energy_cap;
    li_ion_grams_energy(i) = needed_energy_from_li_ion / energy_li_s *
     ↪  1000;
end

total_grams_power = capacitors_grams + li_ion_grams_power;
total_grams_energy = capacitors_grams + li_ion_grams_energy;

figure;
hold on;
plot(capacitors_grams/1000, total_grams_power/1000);
plot(capacitors_grams/1000, total_grams_energy/1000);
legend("Total Weight limited by Power", "Total Weight limited by Energy");
xlabel("Total Weight Capacitors [kg]");
ylabel("Total Weight Energy Storage [kg]");
% title("R = 0.75, a = 2, props = 16");
```

B.3. Battery Pack Calculations

B.3.1. Internal Resistance & Efficiencies

```
clear variables;

am_par_mod = 2;
am_par_cell = 3;
am_ser_mod = 13;
am_ser_cell = 24;
internal_r = 0.0025;

energy = [0.7, 70, 1.3];
eff_prop = [0.7, 0.82, 0.7];
eff_motor = [0.93, 0.93, 0.93];
eff_inv = [0.97, 0.96, 0.97];
eff_dc = [0.98, 0.99, 0.98];
error = [0.95, 0.95, 0.95];

voltage = 883;
power = [530e3, 130e3, 360e3];
current = power./(eff_prop.*eff_motor.*eff_inv.*eff_dc.*error)./voltage;

mod_r = am_ser_cell * internal_r / am_par_cell;
total_r = am_ser_mod * mod_r / am_par_mod;

efficiency = 100 * (1 - (current.^2 .* total_r) ./ (voltage .* current));

power_eff = current.*voltage;
energy_eff = en-
 ↪  ergy./(eff_prop.*eff_motor.*eff_inv.*eff_dc.*error.*efficiency/100);
total_energy = sum(energy_eff) * 77 / 72;
```

B.3.2. Battery Pack Determination

```
clear variables;

nom_v = [2.1, 2.1, 2.3, 2.3, 2.3];  % Nominal voltage of one cell (1.9 -
 ↪  2.6V)
nom_E = [14.7, 19, 33, 33+33*0.2, 33-33*0.2];  % Nominal energy of one
 ↪  cell (14.7 or 19Ah)
nom_P = [2, 6, 7, 7, 7];  % Nominal power (2C or 6C for 30s)
nom_w = [85, 141, 150, 150, 150];  % Nominal weight of one cell (85 or 141
 ↪  g)

max_P = 902e3;  % Maximum power, including efficiencies
max_E = 118e3;  % Needed Energy

V = 800;  % Voltage per motor (max) (400-800V)
A = 105;  % Current per motor (max)
motors = 8;  % Amount of motors

nom_Wh = nom_v .* nom_E;
amount_E = max_E ./ nom_Wh;
nom_W = nom_P .* nom_E .* nom_v;
amount_P = max_P ./ nom_W;
amount_PE = max(amount_E, amount_P);

P = V * A * motors;
amount_V = V ./ nom_v;
amount_A = motors * A ./ (nom_E .* nom_P);
amount_VA = amount_V .* amount_A;

amount = max(amount_PE, amount_VA);
total_weight = amount .* nom_w / 1000;
total_kWh = amount .* nom_Wh / 1000;
Wh_kg = total_kWh ./ total_weight * 1000;

small_parallel = [1, 1, 3, 3, 4];
pack_parallel = [1, 1, 2, 2, 2];
small_series = [1, 1, 24, 24, 24];

total_series = (max_P ./ (small_parallel .* pack_parallel .* nom_E .*
 ↪  nom_P)) / 2.1;
pack_series = ceil(total_series ./ small_series);
pack_V = pack_series .* small_series .* nom_v;
pack_A = pack_parallel .* small_parallel .* nom_P .* nom_E;
pack_w = pack_series .* small_series .* pack_parallel .* small_parallel .*
 ↪  nom_w;
pack_E = pack_series .* small_series .* pack_parallel .* small_parallel .*
 ↪  nom_v .* nom_E;
pack_P = pack_V .* pack_A;
```

B.3.3. Charge Curves

```
clear variables;
close all;

t = 0:1:835;
charge_current = 1115;
V_start = 590;
V_end = 775;
pack_kwh = 142e3;

t_1 = ceil(length(t)*450/charge_current);
t_2 = 100;

time_1 = t(1, 1:t_1);
time_2 = t(1, 1:length(t)-t_1);
time_3 = t(1, 1:t_2);
time_4 = t(1, t_2+1:length(t));

I_1 = repmat(charge_current, 1, length(time_1));
% I_2 = I_1(end) * ((time_2(1)-t_1+100)).^(2) *
 ↪  1./((time_2-t_1+100)).^(2);
I_2 = I_1(end) / (cos(time_2(1)/length(time_2)*3)+1) *
 ↪  (cos(time_2/length(time_2)*3)+1);
I = horzcat(I_1, I_2);

V_1 = V_start + (V_end-V_start) / log(time_1(end)/0.01+1) *
 ↪  log(time_1/0.01+1);
V_2 = repmat(V_end, 1, length(time_2));
V = horzcat(V_1, V_2);

P = I.*V;
E_tot = sum(P)/3600;
E = zeros(1,length(t));
for i = 2:1:length(t)
    E(i) = P(i-1)/3600 + E(i-1);
end

soc = E./pack_kwh;
soc(soc>=1)=1;

figure('Name', 'Current v Voltage');
hold on;
yyaxis left;
plot(t/60, I);
ylabel(”Current [A]”);
ylim([0, charge_current+100]);
yyaxis right;
plot(t/60, V);
ylabel(”Voltage [V]”);
xlabel(”Time [min]”);
ylim([V_start-40, V_end+40]);
xlim([0, length(t)/60]);

figure('Name', 'Power v SoC');
hold on;
```

```
yyaxis left;
plot(t/60,P/1000);
ylabel(”Power [kW]”);
ylim([0, P(t_1)/1000+50]);
yyaxis right;
plot(t/60, soc*100);
ylabel(”SoC [%]”);
xlabel(”Time [min]”);
xlim([0, length(t)/60]);
```

Bibliography

Introduction

[1] Lilium, “An introduction to the lilium jet,” 2019. [Online]. Available: https://lilium.com/jet.

[2] O. Aero, “Blackfly,” 2021. [Online]. Available: https://www.opener.aero/.

[3] Airbus, “Cityairbus,” 2021. [Online]. Available: https://www.airbus.com/innovation/zero-emission/urban-air-mobility/cityairbus.html.

[4] AIAA/IEEE, *Aiaa/ieee eats student design competition*, Nov. 2020.

[5] C. Al Haddad, E. Chaniotakis, A. Straubinger, K. Plötner, and C. Antoniou, “Factors affecting the adoption and use of urban air mobility,” *Transportation research part A: policy and practice*, vol. 132, pp. 696–712, 2020.

Design

[6] W. F. Phillips, “Propeller momentum theory with slipstream rotation,” *Journal of aircraft*, vol. 39, no. 1, pp. 184–187, 2002.

[7] Glenn Research Center. (2021). “The lift equation.”

[8] Airfoil Tools. (2021). “Naca0006.”

[9] M. H. Sadraey, *Aircraft Performance - An Engineering Approach*. CRC Press, 2017, ISBN: 978-1-4987-7655-4.

[10] B. S. U. Ruth Charrondiere David Haytowitz, *Density database version 2.0*, 2012.

[11] A. Batrakov, A. Kusyumov, S. Mikhailov, V. Pakhov, A. Sungatullin, V. Zherekhov, and G. Barakos, “A study in helicopter fuselage drag,” 2012.

[12] T. Stokkermans, D. Usai, T. Sinnige, and L. Veldhuis, “Aerodynamic interaction effects between propellers in typical evtol vehicle configurations,” 2021.

Energy Storage

[13] B. Samaniego, E. Carla, L. O. Neill, and M. Nestoridi, “High specific energy lithium sulfur cell for space application,” 2016.

[14] H. Chen, T. N. Cong, W. Yang, C. Tan, Y. Li, and Y. Ding, “Progress in electrical energy storage system: A critical review,” *Progress in natural science*, vol. 19, no. 3, pp. 291–312, 2009.

[15] M. Mahmoud, M. Ramadan, A.-G. Olabi, K. Pullen, and S. Naher, “A review of mechanical energy storage systems combined with wind and solar applications,” *Energy Conversion and Management*, vol. 210, p. 112 670, 2020.

[16] M. Hedlund, J. Lundin, J. De Santiago, J. Abrahamsson, and H. Bernhoff, “Flywheel energy storage for automotive applications,” *Energies*, vol. 8, no. 10, pp. 10 636–10 663, 2015.

[17] J. Wang, K. Lu, L. Ma, J. Wang, M. Dooner, S. Miao, J. Li, and D. Wang, “Overview of compressed air energy storage and technology development,” *Energies*, vol. 10, no. 7, p. 991, 2017.

[18] J. B. Goodenough and K.-S. Park, “The li-ion rechargeable battery: A perspective,” *Journal of the American Chemical Society*, vol. 135, no. 4, pp. 1167–1176, 2013.

[19] A.-I. Stan, M. Świerczyński, D.-I. Stroe, R. Teodorescu, and S. J. Andreasen, “2014 international conference on optimization of electrical and electronic equipment (optim),” IEEE, 2014, pp. 713–720.

[20] M. Skyllas-Kazacos, M. Chakrabarti, S. Hajimolana, F. Mjalli, and M. Saleem, “Progress in flow battery research and development,” *Journal of the electrochemical society*, vol. 158, no. 8, R55, 2011.

[21] M. Handwerker, J. Wellnitz, and H. Marzbani, “Comparison of hydrogen powertrains with the battery powered electric vehicle and investigation of small-scale local hydrogen production using renewable energy,” *Hydrogen*, vol. 2, no. 1, pp. 76–100, 2021.

[22] Samsung SDI, “What is a solid-state battery?,” 2021.

[23] C. Delbert, “The holy grail is here: A stable, solid-state, lithium-metal battery,” 2021.

[24] M. Horn, J. MacLeod, M. Liu, J. Webb, and N. Motta, “Supercapacitors: A new source of power for electric cars?,” 2018.

[25] X. Meng, Y. Liu, Z. Wang, Y. Zhang, X. Wang, and J. Qiu, “A quasi-solid-state rechargeable cell with high energy and superior safety enabled by stable redox chemistry of li2s in gel electrolyte,” *Energy Environ. Sci.*, vol. 14, pp. 2278–2290, 4 2021. DOI: 10.1039/D0EE03037F.
[26] T. Coombs, “High-temperature superconducting magnetic energy storage (smes) for power grid applications,” pp. 345–365, 2015.
[27] Celsius, “Thermal energy storage,” 2020.
[28] S. Kraemer, “Morocco pioneers pv with thermal storage at 800 mw midelt csp project,” 2020.
[29] Jianghai, *Energy capacitors*, 2019.
[30] OXIS, *Ultra light lithium sulfur pouch cell*, OXIS Energy Ltd, Apr. 2019.
[31] Faraday Institution, *Lithium-sulfur batteries: Lightweight technology for multiple sectors*, Faraday Insights, Jul. 2020.
[32] OXIS, “Oxis energy set to make solid-state lithium-sulfur cell technology a reality,” 2021.
[33] I. A. Hunt, Y. Patel, M. Szczygielski, L. Kabacik, and G. J. Offer, “Lithium sulfur battery nail penetration test under load,” *Journal of Energy Storage*, vol. 2, pp. 25–29, 2015.
[34] Fraunhofer, *High power sic dc/dc converters*, Fraunhofer Institute for Integrated Systems and Device Technology IISB, 2014.
[35] HSR Motors. (2021). “Tesla battery modules > 85-type.”
[36] Panasonic, *Lithium ion panasonic ncr18650b*, Panasonic, 2012.

Charging

[37] H. Lee and A. Clark, “Charging the future: Challenges and opportunities for electric vehicle adoption,” 2018.
[38] T. Blech, “Project chaoji: The background and challenges of harmonising dc charging standards,” 2020.
[39] S. Kim, D. H. Kim, M. Cho, W. B. Lee, and Y. Lee, “Fast-charging lithium–sulfur batteries enabled via lean binder content,” *Small*, vol. 16, no. 47, p. 2 004 372, 2020.
[40] H. Kang, H. Kim, and M. J. Park, “Sulfur-rich polymers with functional linkers for high-capacity and fast-charging lithium–sulfur batteries,” *Advanced Energy Materials*, vol. 8, no. 32, p. 1 802 423, 2018.
[41] J. Guo and J. Liu, “A binder-free electrode architecture design for lithium–sulfur batteries: A review,” *Nanoscale Advances*, vol. 1, no. 6, pp. 2104–2122, 2019.
[42] C. Liu, K. Chau, D. Wu, and S. Gao, “Opportunities and challenges of vehicle-to-home, vehicle-to-vehicle, and vehicle-to-grid technologies,” *Proceedings of the IEEE*, vol. 101, no. 11, pp. 2409–2427, 2013.

BMS

[43] J. Chatzakis, K. Kalaitzakis, N. Voulgaris, and S. Manias, “Designing a new generalized battery management system,” *IEEE Transactions on Industrial Electronics*, vol. 50, no. 5, pp. 990–999, 2003. DOI: 10.1109/TIE.2003.817706.
[44] K. W. E. Cheng, B. P. Divakar, H. Wu, K. Ding, and H. F. Ho, “Battery-management system (bms) and soc development for electrical vehicles,” *IEEE Transactions on Vehicular Technology*, vol. 60, no. 1, pp. 76–88, 2011. DOI: 10.1109/TVT.2010.2089647.
[45] V. Knap, D.-I. Stroe, A. E. Christensen, K. Propp, A. Fotouhi, D. J. Auger, E. Schaltz, and R. Teodorescu, “Self-balancing feature of lithium-sulfur batteries,” *Journal of Power Sources*, vol. 372, pp. 245–251, 2017.
[46] J. Harrison, D. Charles, J. Zenker, and E. Frank, “Using multi-physics system simulation to predict battery pack thermal performance and risk of thermal runaway during evtol aircraft operations,” in *2019 AIAA/IEEE Electric Aircraft Technologies Symposium (EATS)*, IEEE, 2019, pp. 1–13.
[47] A. Fotouhi, D. J. Auger, K. Propp, and S. Longo, “Lithium–sulfur battery state-of-charge observability analysis and estimation,” *IEEE Transactions on Power Electronics*, vol. 33, no. 7, pp. 5847–5859, 2017.
[48] N. Shateri, Z. Shi, D. J. Auger, and A. Fotouhi, “Lithium-sulfur cell state of charge estimation using a classification technique,” *IEEE Transactions on Vehicular Technology*, vol. 70, no. 1, pp. 212–224, 2020.
[49] N. Shateri, D. J. Auger, A. Fotouhi, and J. Brighton, “An experimental study on prototype lithium-sulfur cells for ageing analysis and state-of-health estimation,” *IEEE Transactions on Transportation Electrification*, 2021.